A STUDY OF ROTATIONAL RELAXATION IN A LOW-DENSITY HYPERSONIC FREEJET BY MEANS OF IMPACT-PRESSURE MEASUREMENTS

B. Lefkowitz

July, 1967
Report No. 67-27

Report No. 67-27
July 1967

A STUDY OF ROTATIONAL RELAXATION IN A LOW-DENSITY HYPERSONIC FREE JET BY MEANS OF IMPACT-PRESSURE MEASUREMENTS

B. Lefkowitz

Department of Engineering
University of California
Los Angeles, California

FOREWORD

This report is based upon the dissertation submitted by the author in partial fulfillment of the requirements for the Ph. D. degree in Engineering at UCLA. The research described here was supported chiefly by the National Science Foundation (under Grant GK-580), by the National Aeronautics and Space Administration (under Grant NsG 237-62), and by the UCLA Department of Engineering. Although this study provided basic information, on gas-phase rotational relaxations, which is useful also in other applications (e. g., low-density wind tunnels and rocket exhausts), it was motivated initially by the problem of interpreting data obtained using a molecular beam extracted from a free jet. Hence, this study was part of the continuing program of research involving supersonic molecular beams.

Eldon L. Knuth
Head, Molecular-Beam
Laboratory

TABLE OF CONTENTS

		Page
LIST OF SYMBOLS		iv
LIST OF TABLES		vii
LIST OF FIGURES		viii
ABSTRACT		ix
I.	INTRODUCTION	1
	Motivation for present study	1
	Previous methods and results	3
	Present method	9
II.	APPARATUS	11
	Jet production	11
	Impact-pressure measurement	11
	Range of operating conditions	12
III.	PROCEDURE	15
	Experimental	15
	Data analysis	16
IV.	RESULTS AND DISCUSSION OF RESULTS	25
	Results	25
	Interpretation of results	40
	Comparison with other results	41
V.	SUMMARY OF RESULTS AND CONCLUSIONS	46
	Summary	46
	Conclusions	47
BIBLIOGRAPHY		48

LIST OF SYMBOLS

a	speed of sound
Å	Angstrom (10^{-10} meter)
C_μ	dimensionless coefficient of viscous effect on impact pressure $\left[\equiv \left(p_I^e - p_I^i\right) / \frac{1}{2} \rho v^2\right]$
C_v	specific heat at constant volume
d	diameter
D	sonic-orific diameter
D/Dt	hydrodynamical derivative
h	Planck's constant
k	Boltzmann's constant
K	rotational quantum number neglecting electron spin
Kn	Knudsen number (λ/d)
m	mass per molecule
M	Mach number $\left[\equiv v/(\gamma k T/m)^{1/2}\right]$
n	number density of molecules
N_r	rotational relaxation number
N_2^+	nitrogen ion
$N_2^+ B^2 \Sigma$	upper electronic state of nitrogen ion N_2^+
$N_2 X^1 \Sigma$	ground state of nitrogen molecule
$N_2^+ X^2 \Sigma$	ground state of nitrogen ion N_2^+
p	pressure
r	intermolecular distance
r_M	intermolecular distance at minimum intermolecular potential
Re	Reynolds number $\left[\equiv \rho v d/\mu\right]$

LIST OF SYMBOLS (Continued)

s	constant exponent in viscosity-temperature law $\mu \sim T^s$
T	temperature (absolute)
v	hydrodynamic (average) speed in free jet
V	intermolecular potential
x	distance from source orifice
x'	distance from effective source to standoff shock
X	effective source location
Z	kinetic collision frequency
α	initial inclination of free-jet boundary
γ	specific-heat ratio
δ	distance from tip of pitot tube to standoff shock
Δ	change in rotational energy mode
ϵ	minimum value of intermolecular potential
λ	mean free path
μ	coefficient of viscosity
ρ	density
σ	intermolecular distance at which the intermolecular potential is zero
τ	relaxation time
Ω_μ	viscous cross section factor

Subscripts

o	stagnation conditions
1	upstream of standoff shock
2	downstream of standoff shock
s	static
I	impact
b	background
p	probe

LIST OF SYMBOLS (Continued)

D	sonic
r	rotational
t	translational
v	vibrational
m	Mach disk
f	freezing point
*	effective
e	experimental
i	ideal

LIST OF TABLES

		Page
Table I	Results of Typical Impact-Pressure Survey for Nitrogen	26

LIST OF FIGURES

Figures		Page
1	Schematic diagram of a typical highly underexpanded free jet and qualitative curves of temperature and entropy variations along the free-jet axis	2
2	Mach-number distribution along jet axis	8
3	Schematic diagram of experimental apparatus; detailed drawings of nozzle, stagnation chamber, and pitot tube	13
4	Correction for shock detachment at probe	18
5	Correction for boundary layer in nozzle throat ...	19
6	Correction for location of effective source	20
7	Pressure coefficient C_μ versus probe Reynolds number (effects of rotational relaxation absent) ...	23
8	Impact-pressure correction data (effects of rotational relaxation absent)	24
9 - 16	Impact-pressure ratio p_I^e/p_I^i versus probe Reynolds number (effects of rotational relaxation included). .	27-34
17	Freezing-point distance $(x'/D^*)_f$ versus dimensionless freezing-point parameter $(D^*/\tau_{ro} a_o)$	36
18	Temperature dependence of the collision cross section for molecules whose centers approach to 0.993 σ or less	39

ABSTRACT

A hypersonic free jet of nitrogen was probed using a pitot tube. The impact pressure was found to deviate from predictions of inviscid theory for free jets (after corrections for shock detachment, nozzle boundary layer, and viscous effects at the probe) in regions of rotational nonequilibrium. The rotational relaxation time was inferred from the impact-pressure data by the use of the criterion for sudden freezing $\left|\frac{DT}{Dt}\right| = \frac{T}{\tau_r}$.

The observed relaxation time was interpreted using a relaxation model in which N_r is constant with value unity over the range from 10^{o}K to 100^{o}K and a collision frequency which includes only those collisions for which $r \leq 0.993\sigma$. The temperature dependence of the collision frequency for this model is significantly different than the rate based on a viscosity cross section.

CHAPTER I

INTRODUCTION

1. Motivation for present study

Interest in internal-relaxation-time effects developed as early as 1904, when Jeans[1] derived an expression for the rotational-relaxation time of a system of loaded spheres. The relaxation-time effect was first observed experimentally in 1925 by Pierce[2] who measured the velocity of sound in carbon dioxide as a function of frequency. The resulting velocity dispersion could be explained only by a lag in the adjustment of vibrational energy. The greatly enlarged studies of ultrasonic absorption and dispersion, particularly by the authors cited in References 3, 4, 5, have provided since then an abundance of relaxation data.

More recently, interest in expanding flows, brought about by such applications as sources for high-intensity molecular beams,[6] has motivated studies of effects of relaxation time on gas flows. The first investigator to observe internal (vibrational) relaxation effects in a subsonic free jet was Kantrowitz.[7] Later Huber and Kantrowitz[8] studied rotational relaxation effects in subsonic free jets of water vapor, hydrogen, and nitrogen. Consider a hypersonic free jet exhausting from a sonic nozzle into a low-pressure region. The general structure of such a jet is shown in Figure 1. Reis[9] has made extensive impact-pressure surveys of a hypersonic free jet of nitrogen and found reasonable agreement with inviscid theory close to the nozzle. At lower densities, the measured impact pressure appeared to exceed that predicted by inviscid theory. The rapid decrease of temperature and density in such a flow, and a corresponding increase in the relaxation time, makes adjustment of the lagging energy mode

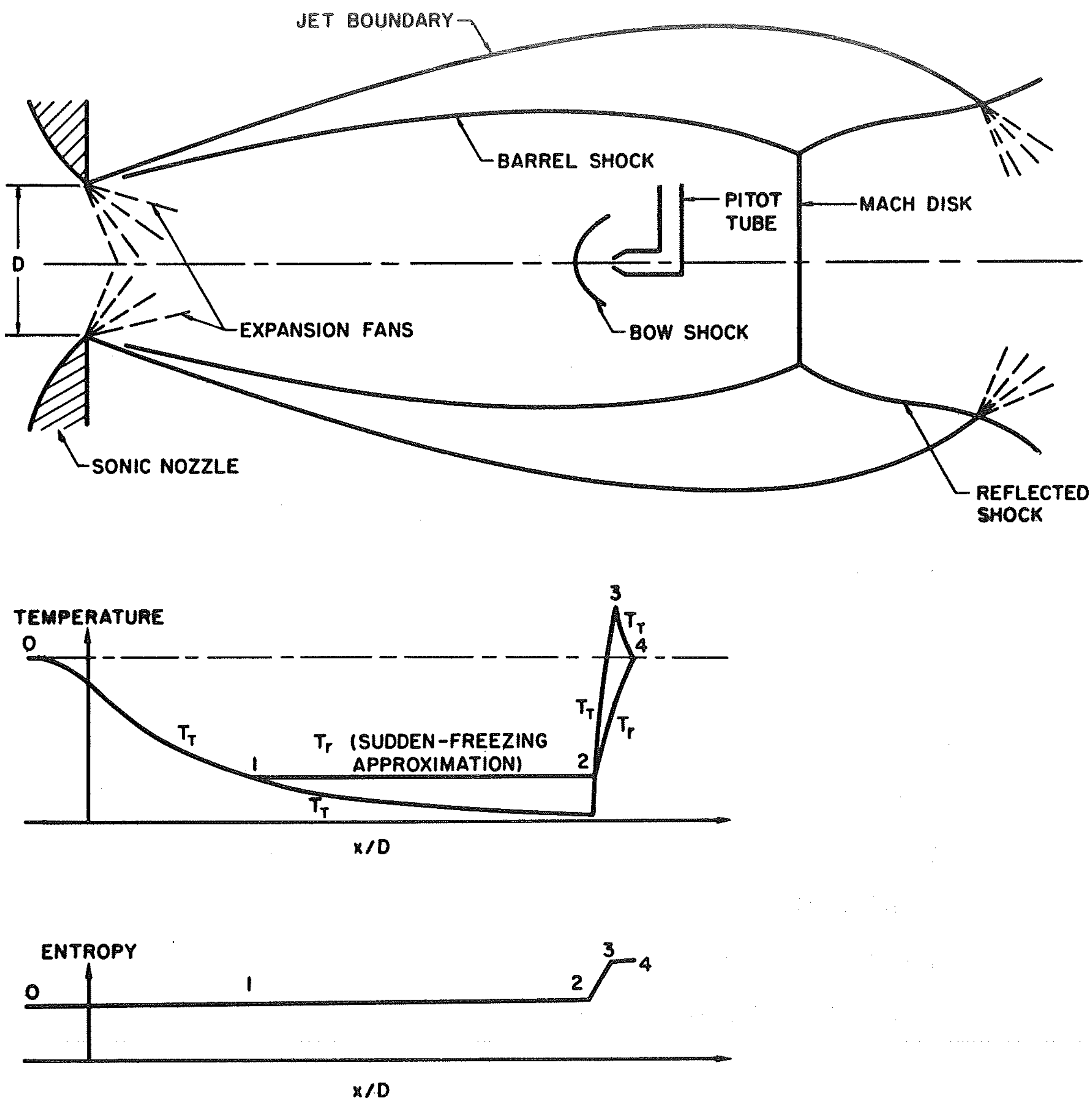

SCHEMATIC DIAGRAM OF A TYPICAL HIGHLY UNDEREXPANDED FREE JET AND QUALITATIVE CURVES OF TEMPERATURE AND ENTROPY VARIATIONS ALONG THE FREE-JET AXIS

FIGURE 1

increasingly difficult. Consequently at some point in the flow the energy in the lagging mode will remain frozen at a value which is higher than the equilibrium value. Knuth[10, 11] proposed that the impact-pressure measurements were affected by rotational freezing, and described how this effect may be used profitably to obtain the rotational-relaxation time. The effect of freezing on the flow properties along the jet axis (in particular, on the impact pressure as measured by a pitot tube) is the concern of the present research.

2. Previous methods and results

Most of the rotational-relaxation-time data has been obtained using ultrasonic acoustic techniques. If the product of the sound frequency and the relaxation time are of order unity, then dispersion results. Measurements of the velocity of sound over frequencies in the dispersion region are used to determine the rotational relaxation time. A difficulty results from the fact that at frequencies comparable to the rotational relaxation frequency, translational dispersion also may occur. A more complete description of these phenomena may be found in Reference 3.

These ultrasonic acoustic studies have been complemented by shock wave studies, which are capable of yielding high-temperature relaxation data. Broadening of the shock thickness due to rotational relaxation can be measured experimentally, thereby providing a method of obtaining rotational-relaxation times.[3]

In a third method, measurement of the internal-energy distribution of the molecules is facilitated by exciting the rotational band spectra by an electron beam. In order for the method to be useful, a relatively strong emission line must be observable as a result of the electron bombardment.[12] For low-pressure nitrogen, strong emission is from the 0-0 vibrational transition of the first negative system of N_2^+. The excitation-emission path considered by Muntz as the most probable is.[13]

$$N_2\,X^1\Sigma \rightarrow N_2^+\,B^2\Sigma \qquad \text{excitation}$$

$$N_2^+\,B^2\Sigma \rightarrow N_2^+\,X^2\Sigma \qquad \text{emission}$$

High-energy electrons excite and ionize the ground-state molecule. The following rapid decay to the ground-state ion gives rise to the first negative system. With the appropriate mathematical model, the line intensities in the first negative system may be predicted, and the rotational temperature obtained from the measured intensities. A model which assumes that the rotational distribution remains unchanged during electron bombardment yields reasonable agreement with spectra obtained at room temperature. At lower temperatures, changes in the rotational distribution which occur during excitation must be considered. To account for these changes Muntz proposes that the rotational levels of the $N_2^+\,B^2\Sigma$ state are populated by direct excitation from the $N_2\,X^1\Sigma$ state according to the optical selection rule $\Delta K = \pm 1$. A possible source of error may be due to the neglected effect of secondary electrons (those produced by beam electrons in ionizing N_2). The application of Muntz's techniques to the study of a free jet has been reasonably successful. A difficulty in the method arises however from the fact that the populations of the higher rotational levels inferred from measurements appear to be greater than those predicted for a Boltzmann distribution. Most investigators neglect the higher rotational levels when inferring a rotational temperature. Marrone[14] has obtained extensive spectral data by probing a free jet of N_2. Rotational temperatures are derived, using Muntz' s model, for a wide range of the parameter $(p_o D)$. As $(p_o D)$ is increased the rotational temperature follows the isentropic curve further downstream before reaching its asymptotic limit. The data showed low scatter and were considered suitable for obtaining freezing-point data (see Chapter IV). Although Marrone's results agree qualitatively with those of Roben and Talbot (Reference 15; a simplified version of Muntz' s model was used), the latter investigators observed a somewhat higher rotational temperature for similar $(p_o D)$. Since their data lie consistently above the isentropic curve, these data are assumed to be in error and are adjusted so that they correspond with the isentropic values. Muntz' s model has also been used by both Hickman[16] and Yasuhara[17] who measured higher rotational temperatures than Marrone for similar $(p_o D)$ values. In order to avoid the difficulties involved in using Muntz' s model, Hickman suggests a data-reduction method based on a modified excitation process. Hickman proposes that the rotational levels of the $N_2^+ \, B^2 \Sigma$ state are populated by a combination of dipole and quadrupole transitions, which allow ΔK to be ± 1 or ± 3. This model yields rotational temperatures which agree well with the isentropic values. However, the effect of varying $(p_o D)$ was not tested. In summary, rotational-freezing-point data may be obtained using Muntz' s model. Uncertainities in the experimental technique seem responsible for the differing results of various investigators. At present the excitation-de-excitation process is not fully understood.

Tracer techniques, in which trace amounts of a strong radiator, such as a sodium atom, are introduced into the test gas, are used to measure the vibrational temperature of a gas. Hurle, Russo, and Hall[18] used this method to study the freezing of the vibrational temperature when high temperature nitrogen ($\sim$ 2300°K) is expanded in a nozzle.

Molecular-beam methods also provide an effective means of exploring the free jet. A molecular beam is skimmed from the free jet and the speed distribution of the beam is measured by a time-of-flight technique.[11, 19] Miller[20] used this approach to observe the lagging of rotational energy in a two-dimensional free jet of nitrogen. The rotational temperature was obtained from an energy balance and the critical assumption that the flow is adiabatic. He carefully examined the various factors which would effect the adiabaticity of the jet, namely probe interaction, background effects in the nozzle chamber, and a nonisotropic temperature distribution. The rotational-relaxation time was obtained then from the equation $\frac{DT_r}{Dt} = \frac{(T_T - T_r)}{\tau_r}$.

Campargue[21] defines a beam-optimization parameter for high intensity molecular beams, shows that this parameter depends on α (therefore on γ), and deduces the rotational freezing of hydrogen upstream of the throat section of a conical converging nozzle from the effective γ. The effect of rotational-energy lag in hydrogen on the lateral dimensions of the barrel shock also has been noted.[22]

Measurement of static pressure has been used to obtain vibrational relaxation data for a high enthalpy nozzle flow.[23]

Huber and Kantrowitz[7, 8] were the first investigators to measure the rotational relaxation time using the subsonic-jet method. A gas is allowed to expand from a chamber through a nozzle in a time which is long compared with the rotational relaxation time, so that the flow remains in equilibrium. The subsonic jet then is compressed at the end of an impact tube in a time much smaller than this relaxation time. The loss of stagnation pressure resulting from the irreversible adjustment following the compression is a measure of the energy lag in the gas.

An impact pressure tube also provides a straightforward method of probing a supersonic free jet. The axial Mach-number distribution may be obtained from the measured impact-pressure distribution if one assumes that the flow is isentropic upstream and downstream of the bow shock on the probe and that the normal-shock relations apply. Measured values are compared with values predicted neglecting relaxation effects. The variation of Mach number along the jet axis was first predicted by Owen and Thornhill[24] for $\gamma = 1.4$ using the method of characteristics. See Figure 2. They considered the inviscid flow from a nearly sonic orifice into a vacuum. Their results also apply to the isentropic core of the free jet bounded by the barrel shock and the Mach disc, in which core the Mach number distribution is independent of the background pressure. Ashkenas and Sherman[25] present (for specific heat ratios of 5/3, 7/5 and 9/7) formulae for predicting Mach numbers and impact pressures based on the more recent characteristics calculations of Woolff. Agreement between the ideal free jet (characteristics solution) and the actual behavior of supersonic free jets has been observed,[25,26,27] provided that the density of the free jet is not so low that the jet core is permeated by the background gas.

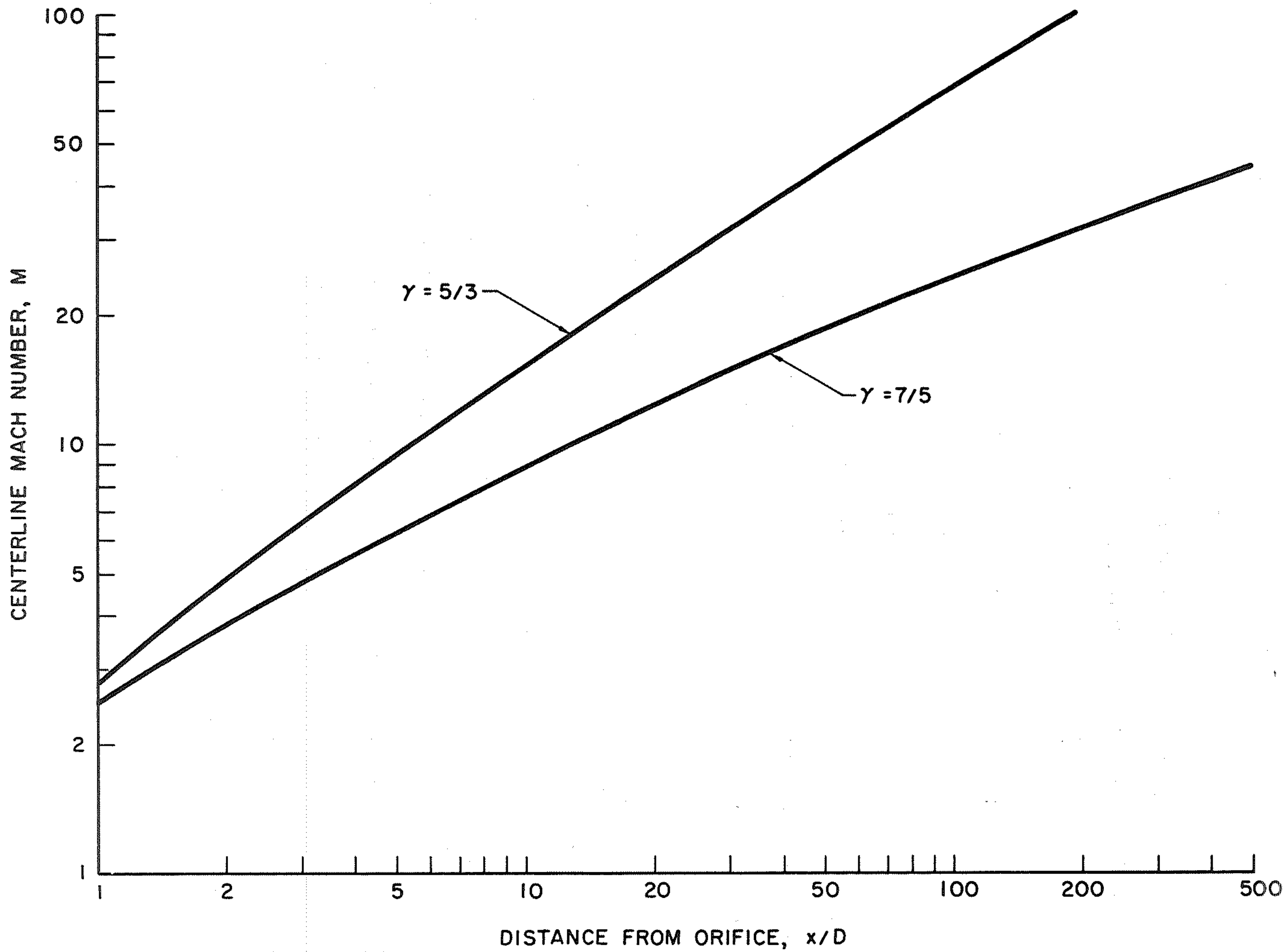

MACH-NUMBER DISTRIBUTION ALONG JET AXIS

FIGURE 2

3. Present method

In the expansion (or compression) of a relaxing gas, a transition region may exist through which the gas departs abruptly from equilibrium. Stollery and Smith[28] have determined the vibrational temperature variation for a gas expanding through a hypersonic nozzle. A transition region is observed which links a flow which is nearly in equilibrium to one in which the vibrational temperature remains nearly constant. The length of the transition region is small compared with the length of the nozzle. The observation of these features has led to the freezing-point approximation used successfully to study the freezing of dissociational (Reference 29) and vibrational (Reference 30) energy. In this approximation, the flow is assumed to be in equilibrium until it reaches a point at which freezing occurs, after which the flow remains frozen.

The freezing point for rotational energy (for a constant rotational heat capacity) is defined as the point at which $\left|\frac{DT}{Dt}\right| = \frac{T}{\tau_r}$. This freezing criterion is similar to criteria used originally to predict the freezing of dissociational and vibrational energy. The rotational freezing point corresponds to the point in the expansion where the measured impact pressure begins to deviate from its isentropic value. Rotational freezing in a supersonic free jet, for the limiting case where freezing takes place early in the expansion, is expected to increase the impact pressure by as much as 21% (Reference 10), the effective γ after freezing being 5/3. If freezing takes place further downstream, then the energy content of the rotational energy mode and the effect of freezing on the expansion are decreased. The expected increase in impact pressure due to rotational freezing is affected negligibly by the location of the relaxation process (i.e., within the bow shock and/or after the fluid is brought to rest). A diagram showing the temperature and entropy history of the fluid as it expands from stagnation conditions to where it is brought to rest at the probe tip is included in Figure 1. The temperature variation from 1 to 2 is drawn in accordance with the sudden-freezing approximation (refer to preceding paragraph). The bow shock appears as an almost instantaneous compression (2 to 3), with a corresponding translational temperature rise. (The rotational degrees of freedom are not excited immediately at 2.) The final drop in translational temperature (3 to 4) is associated with the conversion of translational to rotational energy. The entropy is constant upstream of the bow shock. (In the sudden freezing approximation, no irreversible energy exchange occurs upstream from the bow shock.) Entropy increases across the shock due to the irreversible compression and from 3 to 4 as a result of the irreversible transfer of energy from translational to rotational degrees of freedom. The major portion of the entropy increase occurs across the shock. This increase in entropy (2 to 3) is less than the corresponding increase occurring in an equilibrium diatomic gas at the same x'/D^*. (In the limit of $T_{rf} = T_o$, the increase in entropy across the shock corresponds to its monatomic-gas value.) As a result, rotational freezing will increase the impact pressure since $\ln p_o/p_I$ is proportional to the entropy change (0 to 4). In summary, the impact pressure data, together with the criterion for rotational freezing $|DT/Dt| = T/\tau_r$, make possible the determination of the rotational relaxation time.

CHAPTER II

APPARATUS

1. Jet production

The basic elements of experimental apparatus consisted of (1) a system for producing a free jet, (2) a traversing mechanism for positioning the jet, and (3) a pitot tube for measuring flow properties.

A schematic diagram of the experimental apparatus, together with diagrams of the nozzle, stagnation chamber assembly, and pitot tube, are shown in Figure 3. The stagnation-chamber assembly (including the nozzle) was positioned with respect to the pitot tube by turning a rotary feed-through leading to a micrometer head through a "bellows" seal. The position of the assembly was recorded by means of a graduated disk dial attached to the feed-through (least count = 0.00007 in.). The stagnation chamber was 5/8 in. in diameter by 3/4 in. in length. The nozzle was a 0.0256 in. orifice with a parabolic contour. Two tygon tubes led to the stagnation chamber from outside the vacuum chamber. One tube led to a Statham diaphragm-type strain-gage pressure transducer, Model No. -PA731TC, 0-2psia, which measured the stagnation pressure. Gas (nitrogen, NGC 99.998% purity; argon, AIRCO 99.997% purity) was fed through the other tube from the pressure regulator on the gas cylinder, and was regulated by two metering valves (Granville Phillips Series-203 variable leak; Nupro-2S).

2. Impact-pressure measurement

The impact-pressure probe was designed to avoid probe-displacement and low-density effects, and to give a reasonable response time. In addition, the external chamfer of the probe must be sufficiently small to insure a proper flow pattern around the probe. Although one would prefer a probe large enough to avoid viscous effects (see Chapter 3), one is limited by the first requirement. The dimensions of the probe were: length, 1/2 in.; O. D., 0.018 in.; I. D., 0.010 in. The response time was estimated, on the basis of work by Schaaf and Cyr,[31] to be 25 sec. Low-density effects were avoided by taking measurements only for pitot-tube Knudsen numbers less than unity. Since the probe tip is blunt, a bow shock, which gradually becomes an oblique shock further from the probe centerline, is formed in front of the probe. An estimate of the allowable chamfer was given then by the maximum angle an oblique shock may deflect the stream lines. A maximum range for the expected Mach numbers was 12^{o}-45^{o} ($\gamma = 7/5$, M = 1.5-15). A 10^{o} external chamfer was chosen. The probe was silver soldered to an adapter tube which was clamped to a shaft fastened to the side flange (Figure 3). The instrumentation for pressure measurement consisted of a Rosemount diaphragm-type capacitive pressure transducer, Model No. 830A5. The probe was equipped with a solenoid valve and the necessary tygon tubing leading to the transducer. Each transducer output was measured by a Leeds and Northrup millivolt potentiometer (Model No. 8662, range 0-75 mv, least count 0.01 mv) with the aid of a supplementary galvanometer (L.N.Model No. 2430A). The calibration standard consisted of a Meriam Model 34H10-TM silocone-oil manometer. The specific gravity of the oil is 0.9122 at 25^{o}c. Under these conditions the least count of the manometer is 0.005 torr.

3. Range of operating conditions

The bulk of the pumping speed was supplied by a Stokes Series-150, 16 in.-diameter, Ring Jet oil-diffusion pump backed

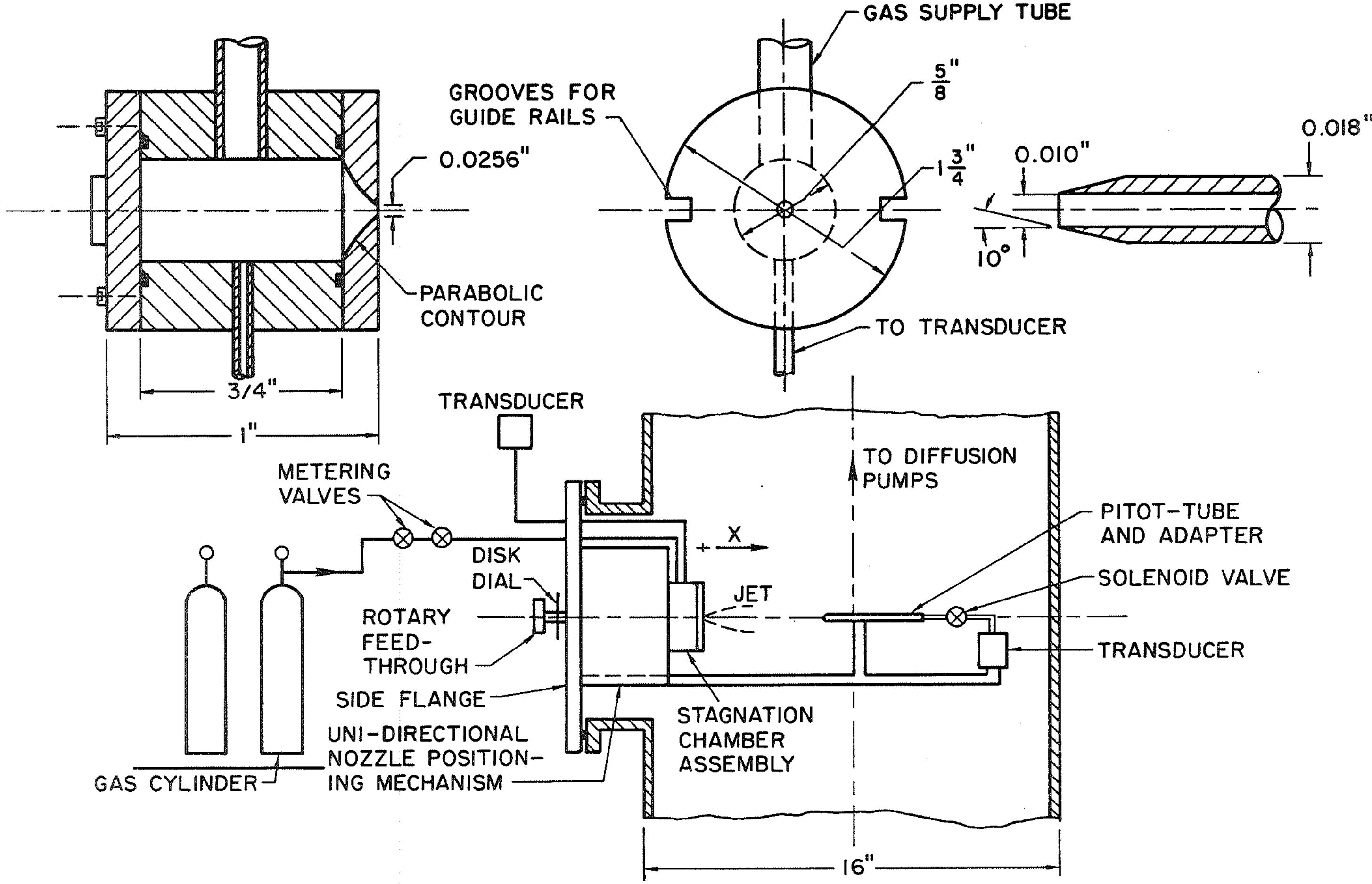

SCHEMATIC DIAGRAM OF EXPERIMENTAL APPARATUS; DETAILED DRAWINGS OF NOZZLE, STAGNATION CHAMBER, AND PITOT TUBE

FIGURE 3

by a Stokes Model 212-H mechanical vacuum pump. An NRC Type-530 Alphatron Vacuum Gage was used to measure the background pressure in the vacuum chamber. (A complete description of the molecular beam instrumentation and apparatus, a segment of which was just described, may be found in Reference 32.) Nozzle source pressures were varied from about 2 to 60 torr. The maximum obtainable pressure ratio p_o/p_b varied from about $.55 \times 10^{-4}$ torr at the lowest source pressure to 4.3×10^{-4} torr at the highest source pressure. For the background pressures encountered, the pumping capacity averaged about 2,300 liters/sec. The source gas was considered to be at room temperature as measured by a mercury thermometer located just outside the vacuum system.

CHAPTER III
PROCEDURE

1. Experimental

Prior to the impact-pressure measurements, the transducers used to measure stagnation and impact pressure were calibrated using the Meriam manometer described in Chapter II.

A typical test run consisted of first aligning the probe with the nozzle axis and then noting the initial nozzle-to-probe setting on the disk dial. The vacuum system was closed then and the vacuum pumps were turned on. After reaching a vacuum of about 2×10^{-4} torr, the output of the capacitive transducer (connected to the probe) was recorded. If the output changed no more than 0.02 mv (corresponding to a pressure of about 1 micron†) in an hour (about 3 days were required for the transducer to stabilize after exposure to atmospheric pressure), the gas was admitted at the desired stagnation pressure. Adequate time was allowed for the probe pressure to reach its equilibrium value. Ten minutes were required generally to complete a reading at one point. During this time, the stagnation pressure was monitored periodically, the drift being approximately 0.01 mv (~ 0.02 torr). A new data point was taken by moving the nozzle from its furthest position closer to the probe. The position of the Mach disk was computed for each run using the relation (see Table 1 in Chapter IV).

$$x_m/D^* = .67\left(p_o/p_b\right)^{1/2} \qquad (1)$$

---

†A 750 Ω resistor was shunted across the output terminals of the transducer which was operated then at 0.1 full scale. This gave an output of about 75 mv at a pressure of 5 torr.

Interference with the Mach disk was avoided by keeping $x'/D^{*} << x_m/D^{*}$. At the end of each run the zero readings of both transducers were checked again. A run was considered satisfactory if the zero drift was less than 0.03 mv (~ 0.003 torr) and 0.10 mv (~ 0.02 torr) for the capacitive and strain gage transducers respectively. A complete run usually required several runs on different days. Impact-pressure surveys were made using both nitrogen and argon at room temperature.

2. Data analysis

If the flow upstream from and downstream from the probe shock is isentropic, then the loss in stagnation pressure, due only to the increase in entropy through this shock and the stagnation pressure ratio, is (Reference 33)

$$\frac{p_I^i}{p_o} = \left[\frac{(\gamma+1)\,M_1^2}{(\gamma-1)\,M_1^2+2}\right]^{\frac{\gamma}{\gamma-1}} \left[\frac{\gamma+1}{2\,\gamma M_1^2 - (\gamma-1)}\right]^{\frac{1}{\gamma-1}} \tag{2}$$

Therefore, once the impact pressure is known, all the flow variables may be calculated. The characteristics calculations of Woolff† were used to define ideal gas properties along the free jet centerline. The ideal impact pressure as tabulated in Reference 34 may be calculated then as a function of x/D using Equation (2). The various corrections which must be applied to the measured data for the proper interpretation and comparison of measured impact pressures with predicted ideal impact pressures (based on Equation (2)) are described here.

---

†The results of these calculations were communicated to me by F.S. Sherman.

If the dimensions of the probe are not small relative to the scale of the flow, then a correction must be applied to the probe position since Equation (2) refers to conditions at the position of the detached shock rather than at the end of the probe. Experimental shock-detachment distances, as a function of Mach number, for a flat-nosed body of revolution and $\gamma = 7/5$ may be found in References 33, 35. The values for the shock-detachment distance predicted by Serbin[35] agree well with measurements and are plotted versus $1/M$ for $\gamma = 5/3$ and $7/5$ in Figure 4.

As a result of boundary-layer growth on the walls of the nozzle, the effective flow diameter which determines the scale of the flow is somewhat less than the geometric value. The effective diameter was determined using a wet test meter (Precision Scientific Co., 1 rev corresponds to 0.250 ft.^{3}) to measure the actual flow rate through the nozzle as a function of stagnation pressure and comparing this flow rate with the ideal flow rate from a sonic nozzle. The effective flow diameter was determined also by adjusting the parameter D^* to provide agreement between the calculated ideal impact pressure and the measured impact pressure. The resulting effective flow diameters are shown in Figure 5. The good agreement between the two methods obtained here cannot be expected in general; differences of about 4% have been noted for a particular nozzle geometry (Reference 36).

An additional correction must be applied to the probe position to account for the difference between the actual and assumed nozzle entry shape. Viscous and vena-contraction effects displace the sonic surface from the exit plane. The effective source location was obtained by forcing a fit of the pitot measurements with the computed curve. The result of this calculation is shown in Figure 6.

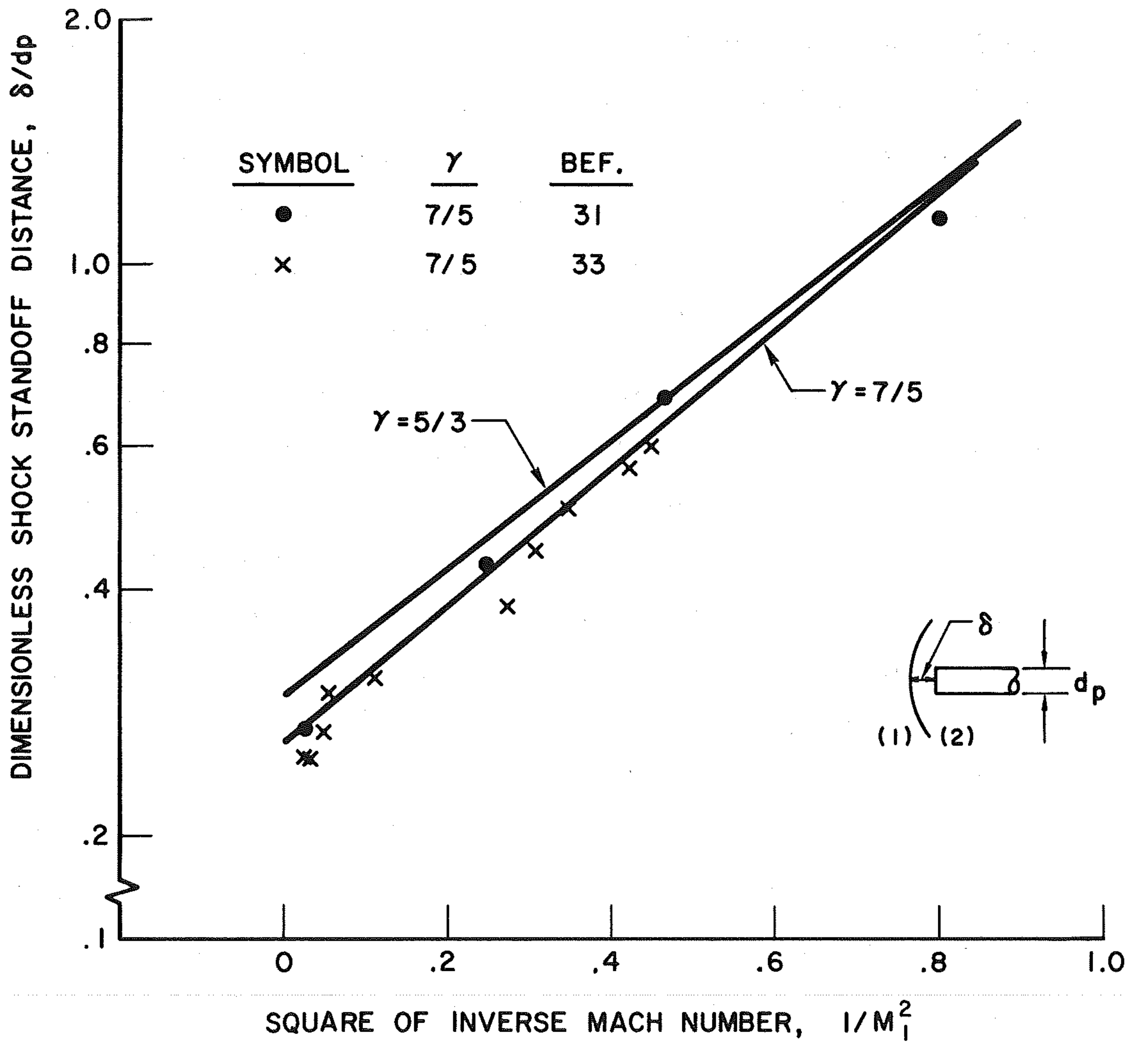

CORRECTION FOR SHOCK DETACHMENT AT PROBE

FIGURE 4

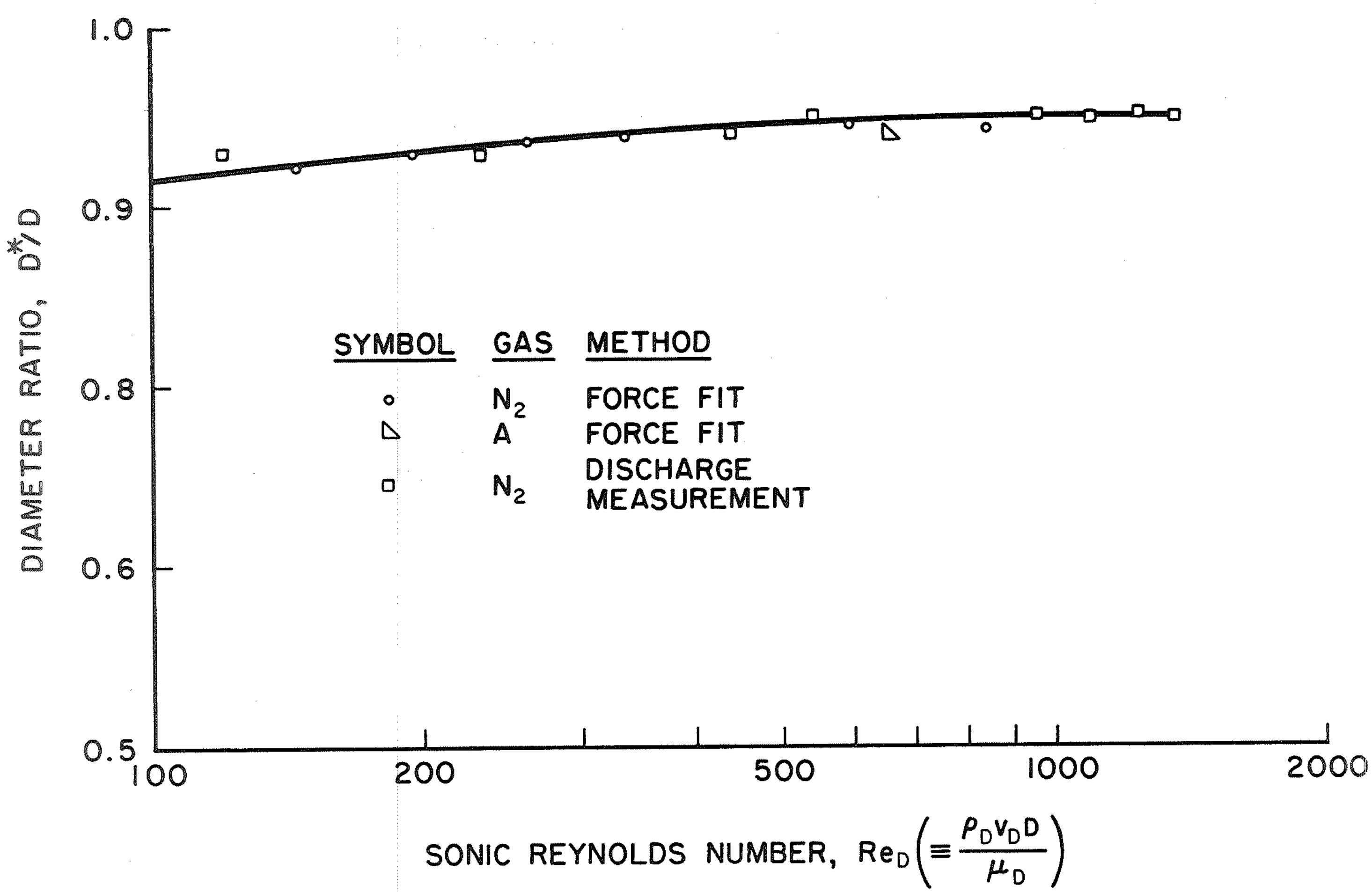

CORRECTION FOR BOUNDARY LAYER
IN NOZZLE THROAT

FIGURE 5

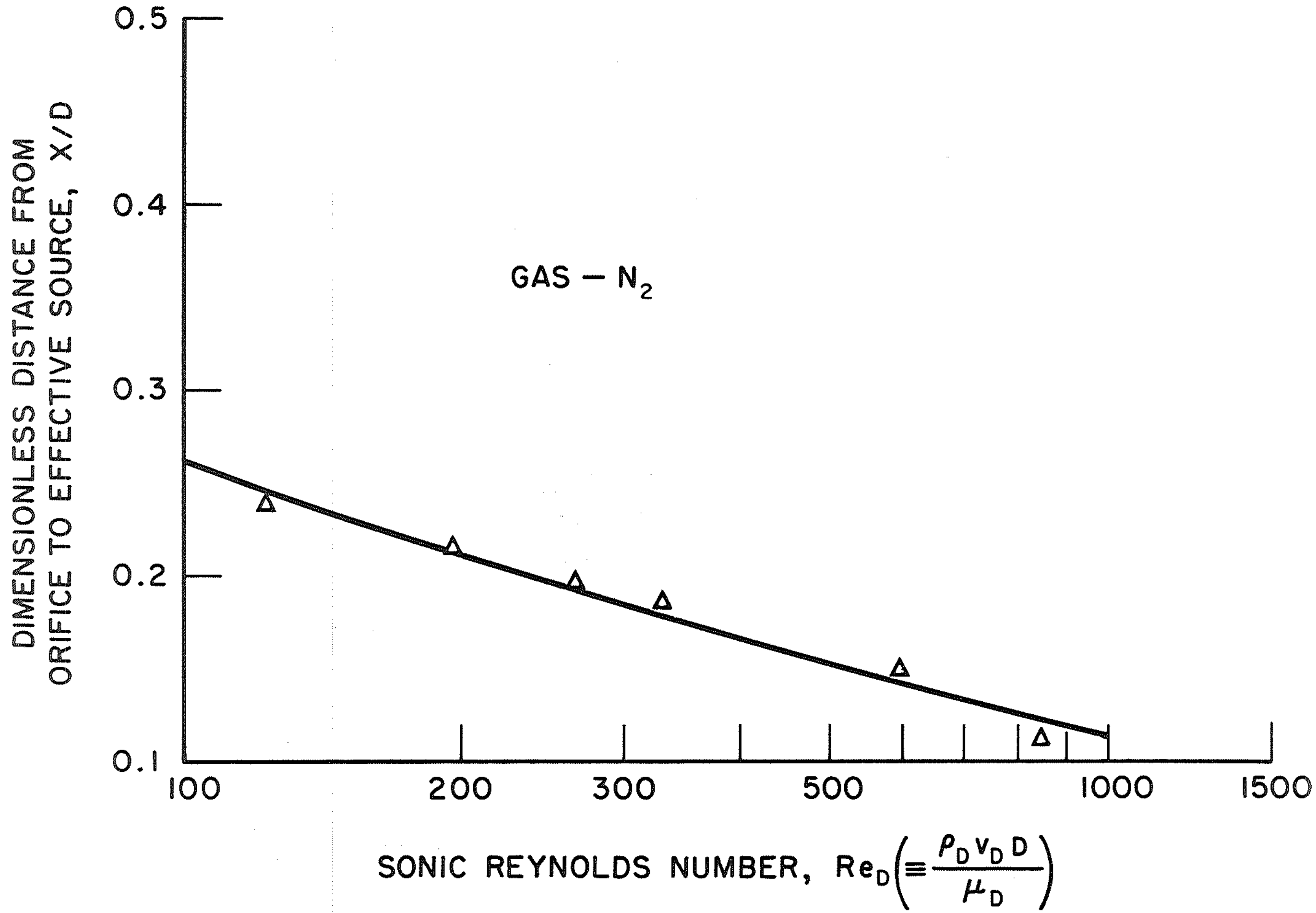

CORRECTION FOR LOCATION OF EFFECTIVE SOURCE

FIGURE 6

At low probe Reynolds number $\left(Re_p \equiv \frac{\rho_2 v_2 d_p}{\mu_2}\right)$ behind the normal shock, based on the probe O. D., impact-pressure readings are influenced by the boundary layer on the probe. Homann[37] showed that, for an incompressible fluid in subsonic flow, the increase in measured impact pressure over the ideal impact pressure is related to the velocity gradient at the stagnation point of the probe. In an extension of Homann's analysis to compressible flows, Chambre[38] predicts that the pressure coefficient $C_\mu\left[\equiv \left(p_I^e - p_I^i\right) / \frac{1}{2}\rho v^2\right]$ should increase with decreasing Mach number. His theory may also apply to probes in supersonic flow if the standoff shock does not interact appreciably with the boundary layer on the probe. Some agreement with theory has been obtained for source shaped probes(Reference 39), but for a particular probe geometry (and wind tunnel) an empirical correlation must be obtained. This was done here in the following manner. Since the measured impact pressure may have been effected by rotational freezing, the ratio of the measured impact pressure and the ideal impact pressures $\left(p_I^e/p_I^i\right)$ was compared for two nitrogen runs made at different stagnation pressures but at the same probe Reynolds number. If a split occurred, the point corresponding to the higher impact pressure ratio $\left(p_I^e / p_I^i\right)$ was assumed to be effected by rotational freezing and was omitted from the correlation. This procedure was continued until a well-defined curve was obtained for a probe Reynolds number range from 1 to 10 (Figure 8). To determine whether this correlation curve actually reflects the effects of viscosity alone, an impact pressure survey was made using argon, for which internal relaxation effects were absent, and compared with the results of several nitrogen runs believed to be free of freezing effects. When comparing impact pressure data for gases with different specific heat ratios, Homann suggests that one should use C_μ rather than p_I^e / p_I^i. (If p_I^e / p_I^i were used, then the argon and nitrogen data would not collapse onto a single curve.) Since the correlation as shown in Figure 7 is satisfactory, the impact-pressure data shown in Figure 8 may be assumed to be free of freezing effects. This curve is referred to as the viscous-correction curve.

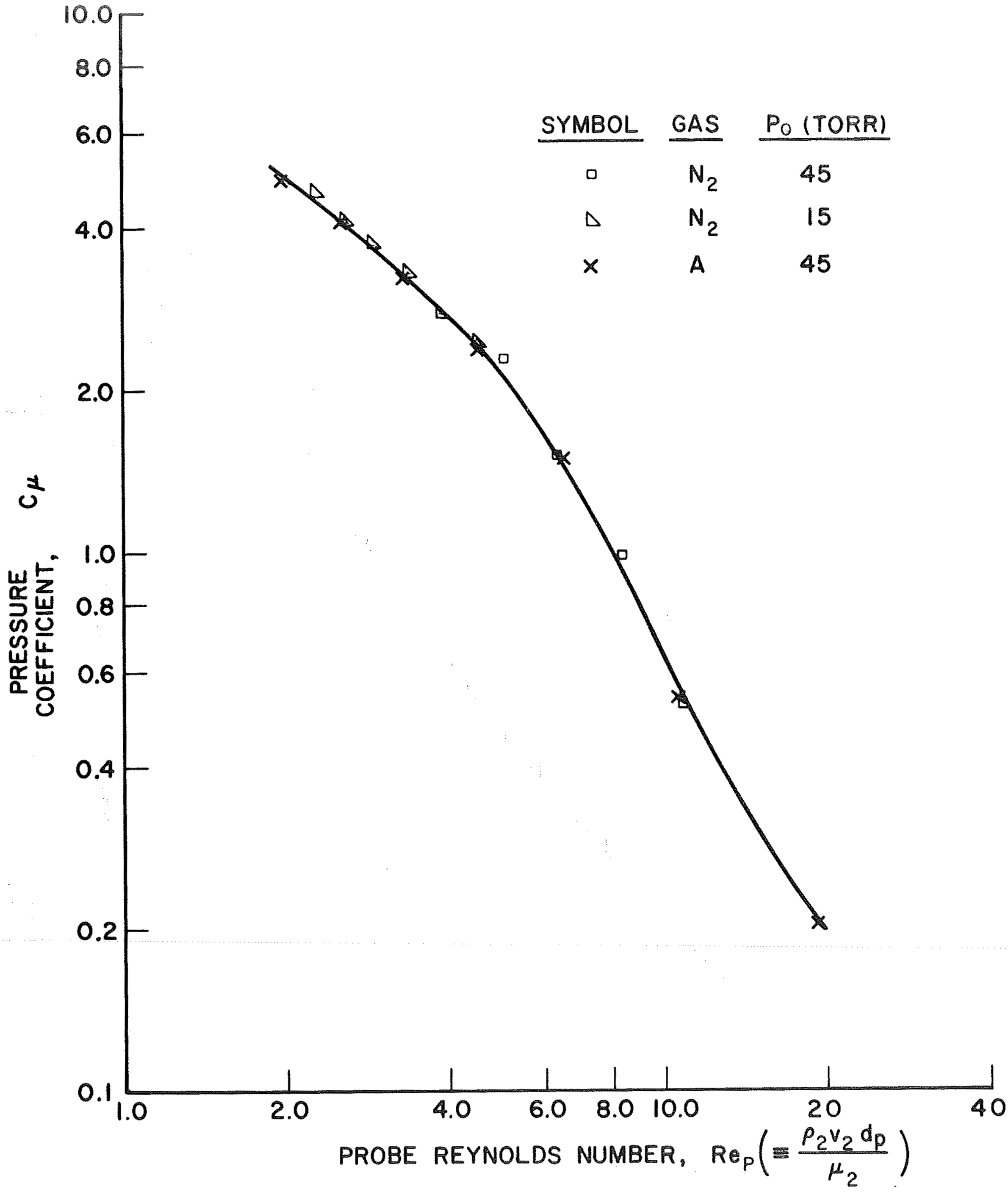

PRESSURE COEFFICIENT C_μ VERSUS PROBE REYNOLDS NUMBER
(effects of rotational relaxation absent)

FIGURE 7

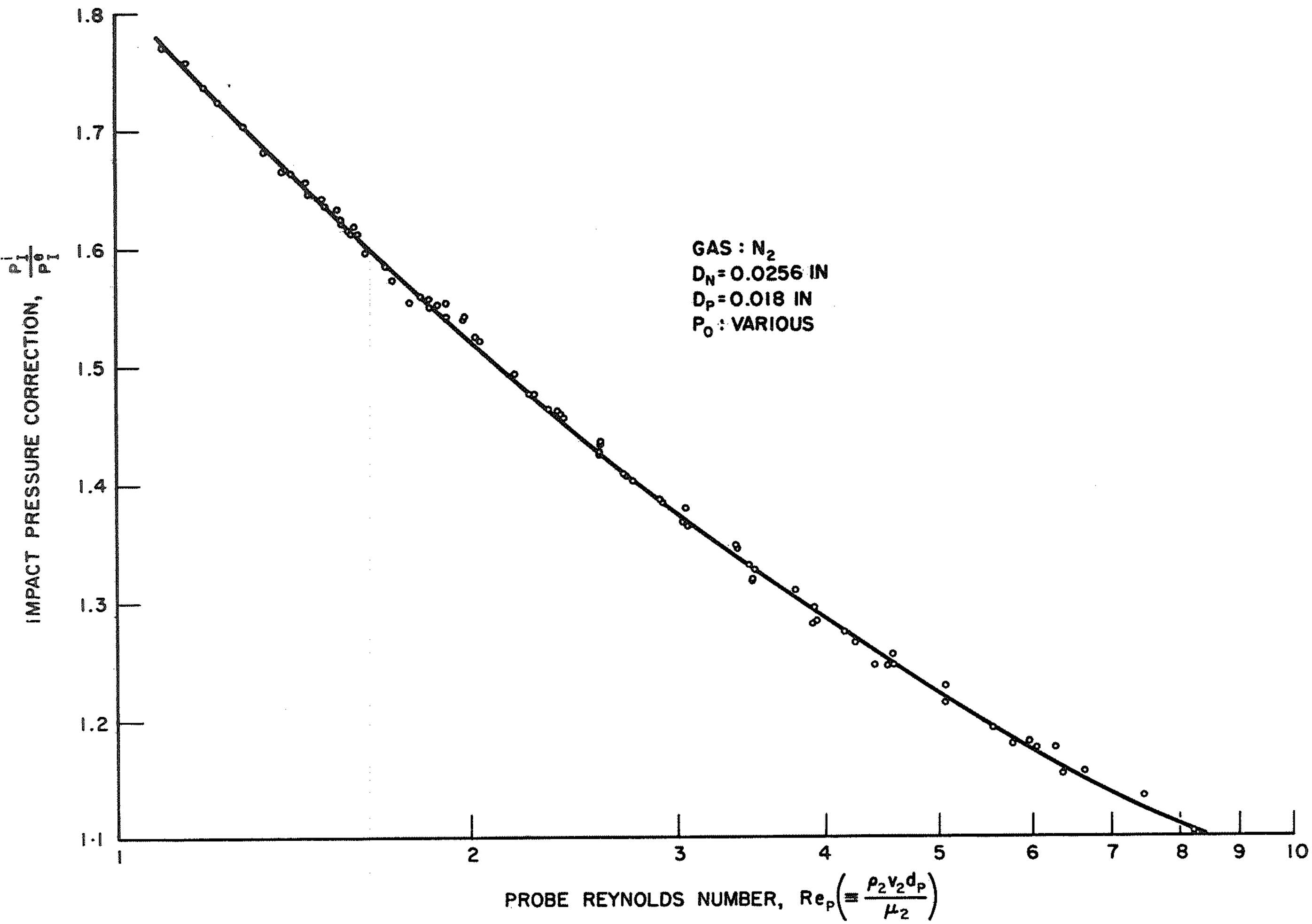

IMPACT-PRESSURE CORRECTION DATA
(effects of rotational relaxation absent)

FIGURE 8

CHAPTER IV

RESULTS AND DISCUSSION OF RESULTS

1. Results

Axial impact-pressure surveys were obtained for nitrogen at room temperature and over a range of stagnation pressure from 2.5 to 60 torr. The results of a typical impact-pressure survey for nitrogen are tabulated in Table 1[†] The experimental results for nitrogen and argon are presented in Figures 7 through 16. Referring to Figures 7 and 8, no Mach-number dependence is observed since the probe Knudsen number $\left(Kn_p \equiv \lambda_2/d_p\right)$ is less than unity for all impact-pressure data taken. The results of an impact-pressure survey for nitrogen at $p_o = 2.5$ torr are shown in Figure 9. The data are seen to follow the curve down to $Re_p = 2.5$ (which corresponds to $x'/D^* = 1.80$). The point at which the data begin to deviate from the viscous correction curve is referred to as the freezing point. As can be seen from Figures 9 - 16, the deviation of points (in the rotational-freezing region) from the viscous correction curve is about 1 to 2%. The deviations indicated in Figures 9 - 16 do not mean, however, that rotational freezing increases the impact pressure only 1 to 2%. Although rotational freezing also increases the probe Reynolds number (by as much as 49% according to the predictions of Reference 10), the probe Reynolds number for Figures 9 - 16 was calculated neglecting effects of rotational freezing. Neglecting effects on probe Reynolds number tends to mask effects on impact pressure.

[†]A complete tabulation of all the impact-pressure data may be obtained from the Molecular Beam Lab.-UCLA, where it is filed.

TABLE I

RESULTS OF TYPICAL IMPACT-PRESSURE SURVEY FOR NITROGEN

RUN # 4

P_o = 15 torr

T_o = 296°K

D^* = .0238 in.

X = .00548 in.

$Re_D = \left[\equiv \frac{\rho_D v_D D}{\mu_D} \right] = 195$

x'/D^*	M	p_I^e/p_o	p_I^i/p_o	p_I^e/p_I^i	$Re_p\left[\equiv \frac{\rho_2 v_2 d_p}{\mu_2}\right]$
3.244	5.075	1.100	.05826	1.258	4.57
3.513	5.282	.969	.04980	1.297	3.91
3.784	5.484	.866	.04286	1.346	3.36
4.054	5.668	.778	.03749	1.383	2.91
4.323	5.844	.709	.03307	1.428	2.57
4.594	6.023	.647	.02918	1.478	2.26
4.863	6.201	.595	.02582	1.536	1.98
5.131	6.380	.548	.02990	1.595	1.76
5.400	6.540	.511	.02060	1.653	1.58
5.669	6.691	.474	.01868	1.689	1.42
5.938	6.830	.442	.01709	1.723	1.30
4.408	5.900	.04574	.03179	1.439	2.46
4.497	5.959	.04450	.03051	1.459	2.36
4.917	6.238	.03891	.02518	1.545	1.94
4.972	6.273	.03822	.02460	1.544	1.90
5.022	6.308	.03763	.02402	1.567	1.85
5.077	6.345	.03708	.02344	1.582	1.79
5.131	6.380	.03638	.02290	1.589	1.76
5.215	6.436	.03554	.02213	1.606	1.70
5.304	6.486	.03465	.02135	1.623	1.63
4.497	5.959	.0446	.03051	1.457	2.36
4.657	6.065	.04215	.02835	1.487	2.18
4.690	6.088	.04173	.02790	1.496	2.15
4.720	6.108	.04134	.02752	1.502	2.12
4.745	6.122	.04096	.02726	1.503	2.11
4.766	6.138	.04074	.02696	1.511	2.08
4.787	6.150	.04050	.02674	1.515	2.07
3.784	5.484	.05762	.04286	1.344	3.36
4.054	5.688	.05204	.03749	1.388	2.91
4.323	5.844	.04709	.03307	1.424	2.57
4.594	6.023	.04314	.02918	1.478	2.26
4.863	6.201	.03955	.02582	1.532	1.98
5.131	6.380	.03650	.02290	1.594	1.76
5.400	6.540	.03383	.02060	1.642	1.58
5.669	6.691	.03153	.01868	1.688	1.42
5.938	6.830	.02949	.01709	1.726	1.30

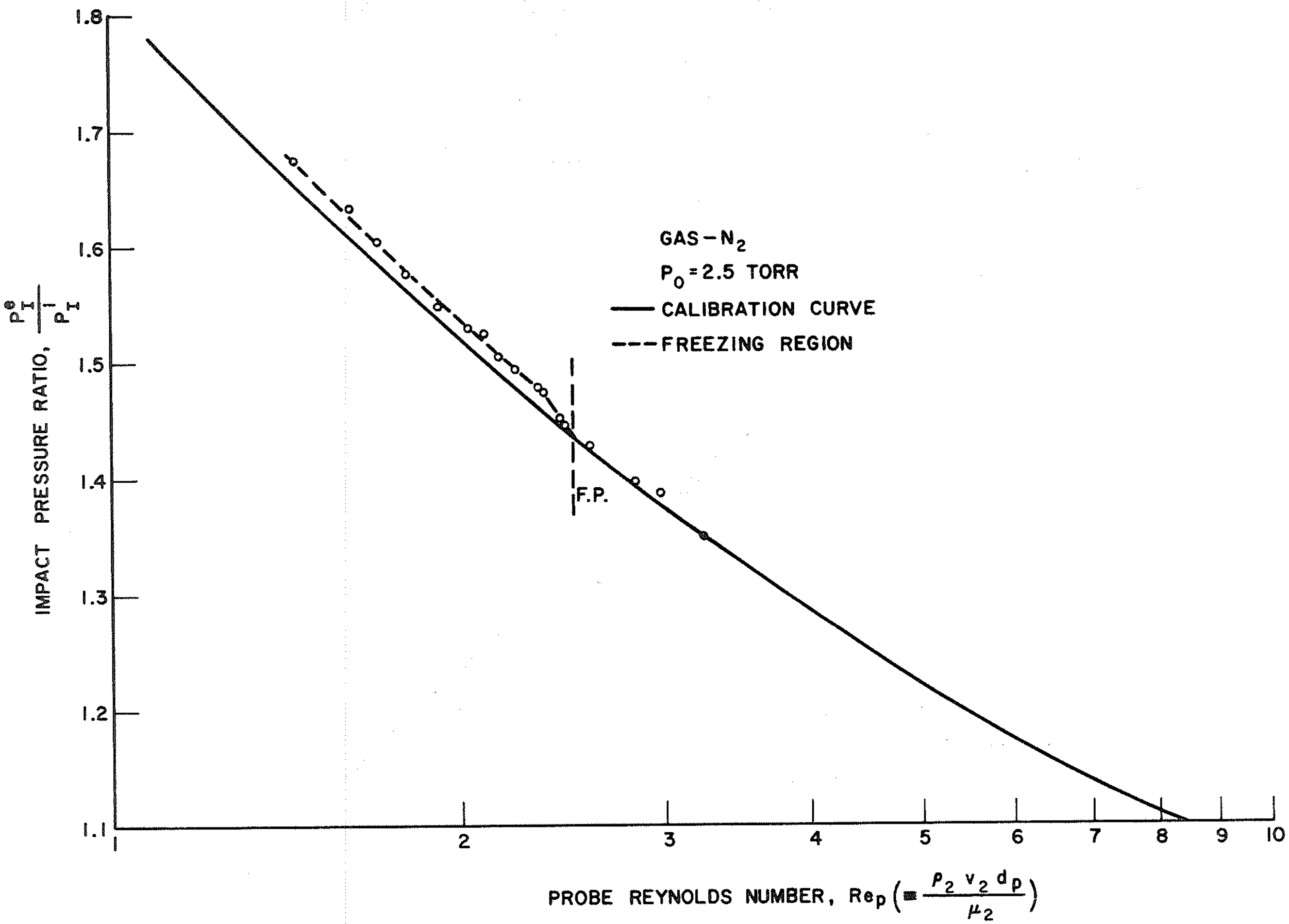

IMPACT-PRESSURE RATIO p_I^e/p_I^i VERSUS
PROBE REYNOLDS NUMBER
(effects of rotational relaxation included)

FIGURE 9

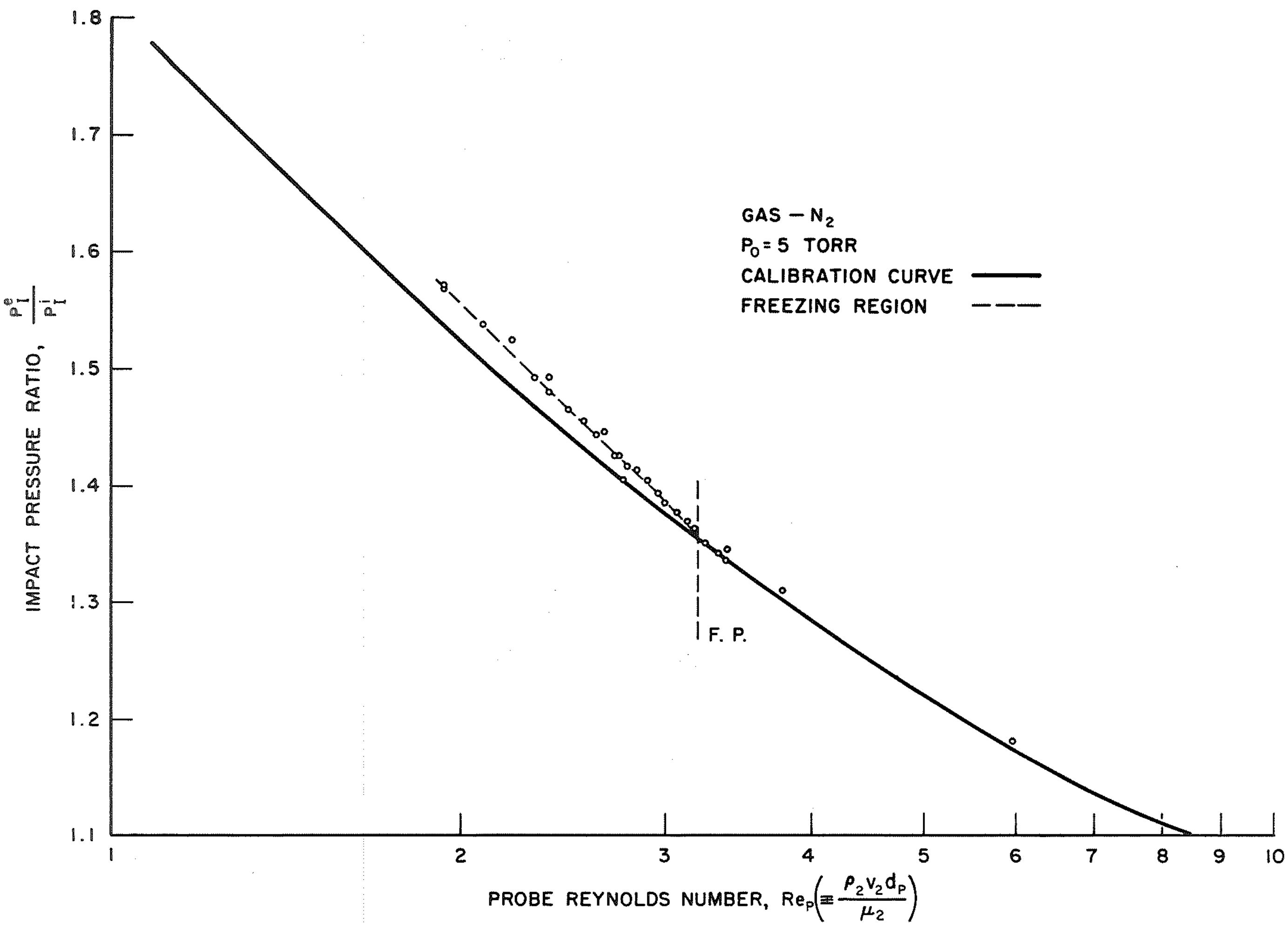

IMPACT-PRESSURE RATIO p_I^e / p_I^i VERSUS PROBE REYNOLDS NUMBER
(effects of rotational relaxation included)

FIGURE 10

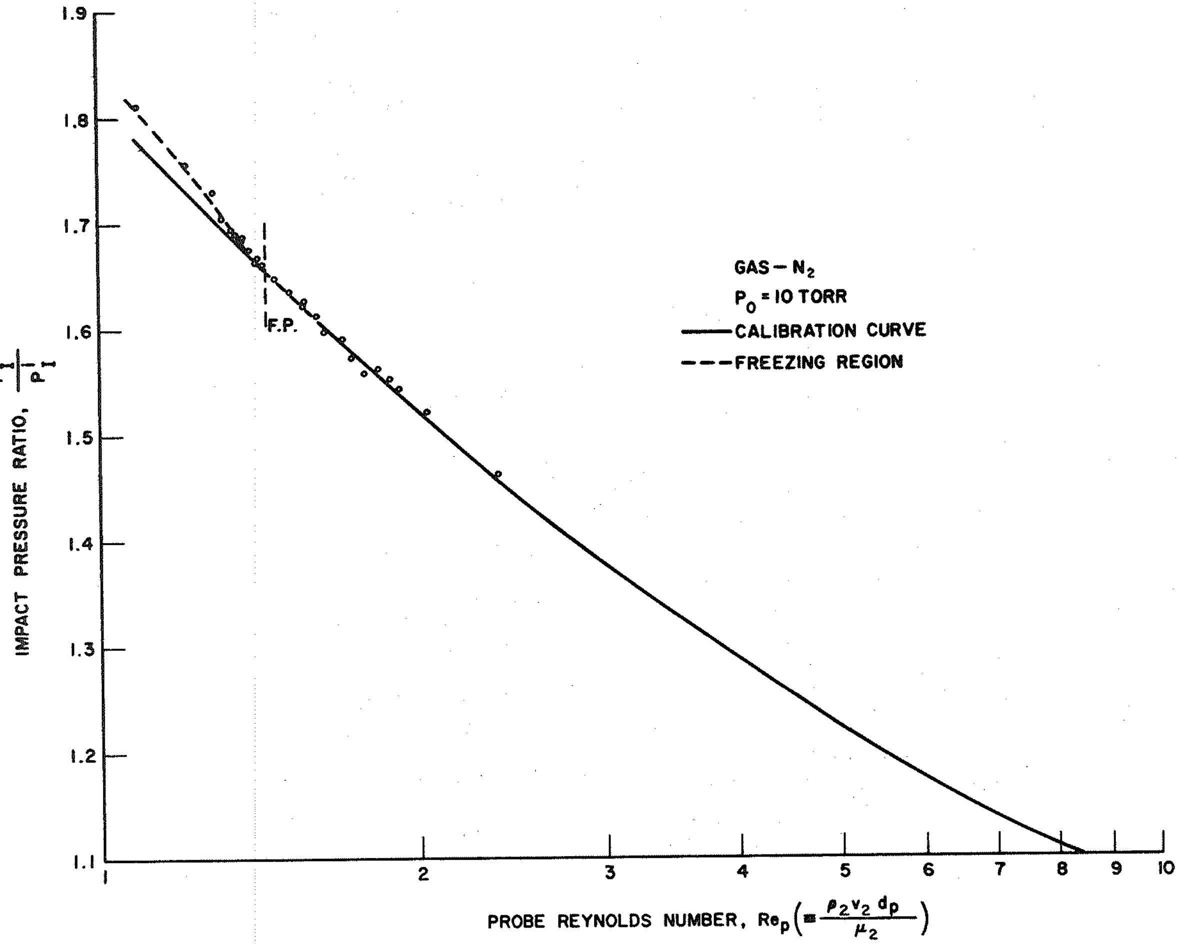

IMPACT-PRESSURE RATIO p_I^e / p_I^i VERSUS
PROBE REYNOLDS NUMBER
(effects of rotational relaxation included)

FIGURE 11

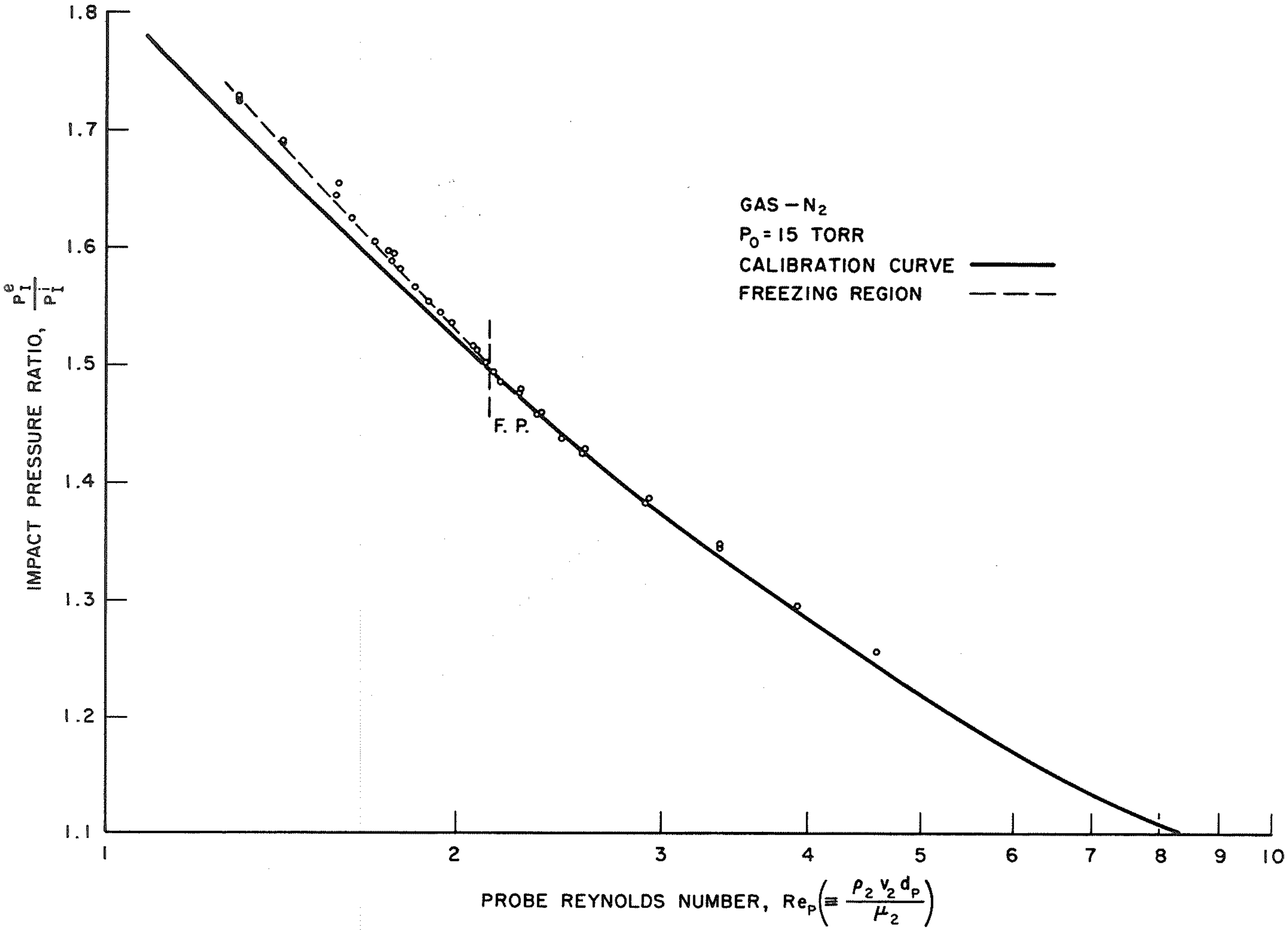

IMPACT-PRESSURE RATIO p_I^e/p_I^i VERSUS
PROBE REYNOLDS NUMBER
(effects of rotational relaxation included)

FIGURE 12

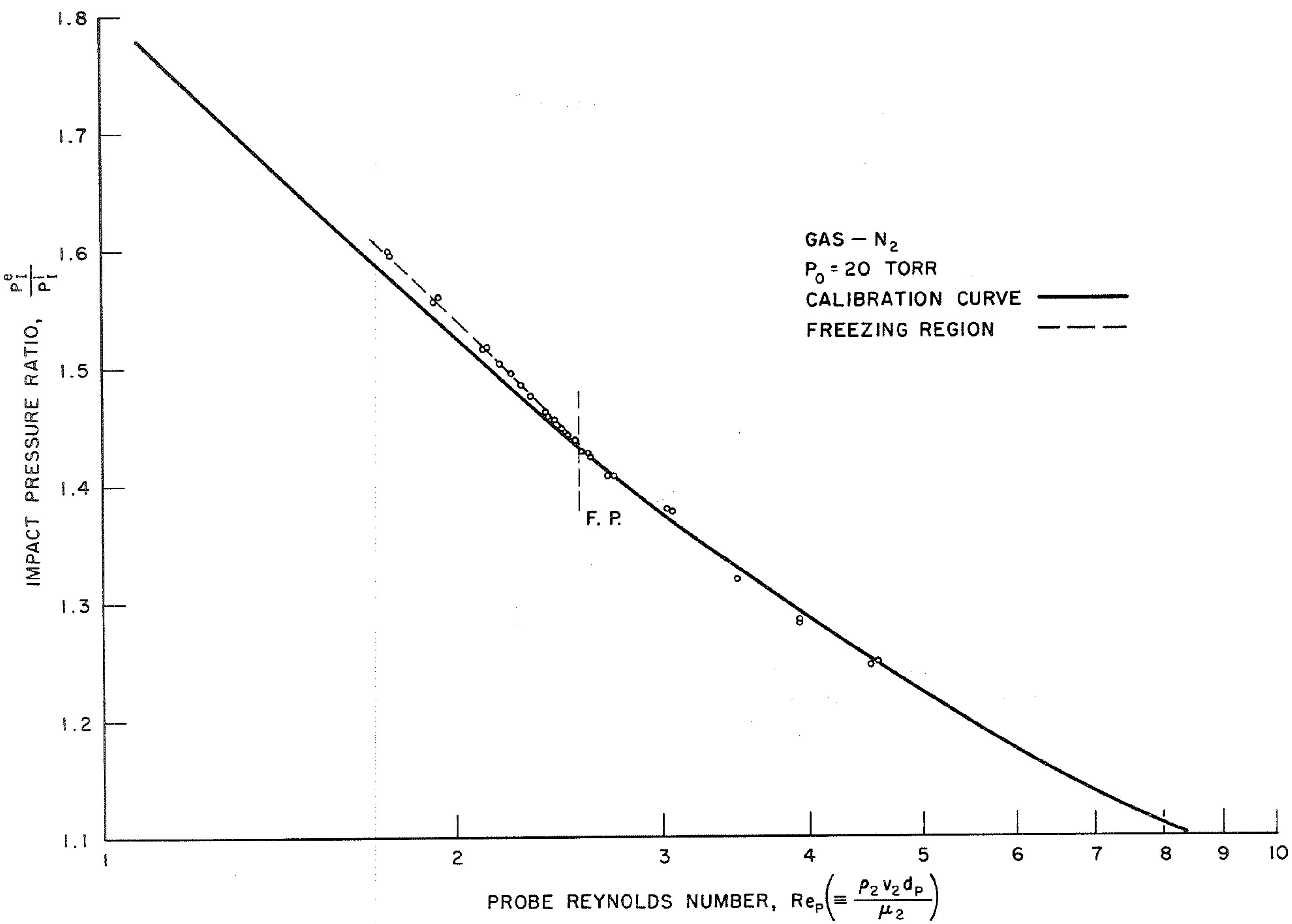

IMPACT-PRESSURE RATIO p_I^e/p_I^i VERSUS PROBE REYNOLDS NUMBER
(effects of rotational relaxation included)

FIGURE 13

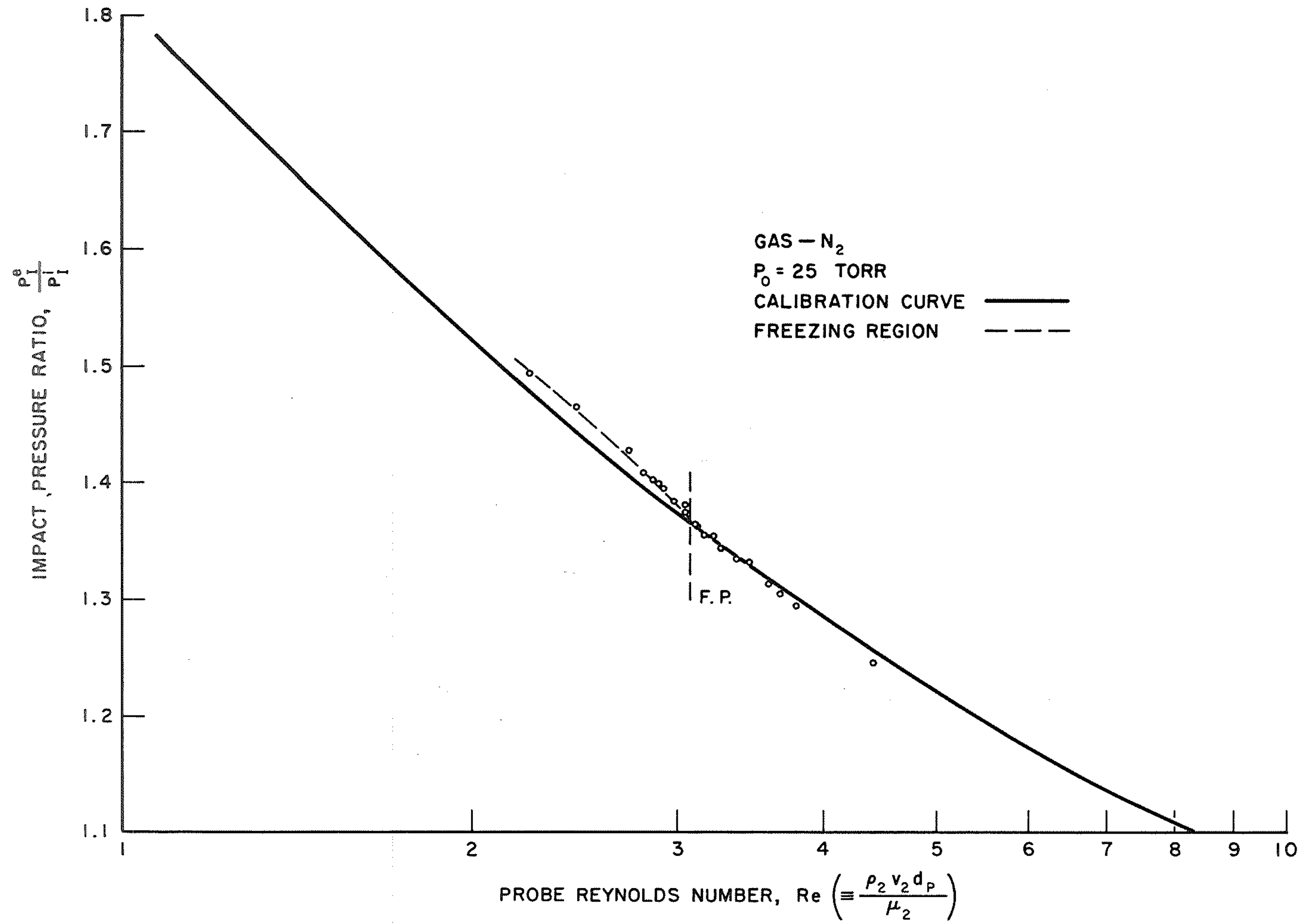

IMPACT-PRESSURE RATIO p_I^e/p_I^i VERSUS PROBE REYNOLDS NUMBER (effects of rotational relaxation included)

FIGURE 14

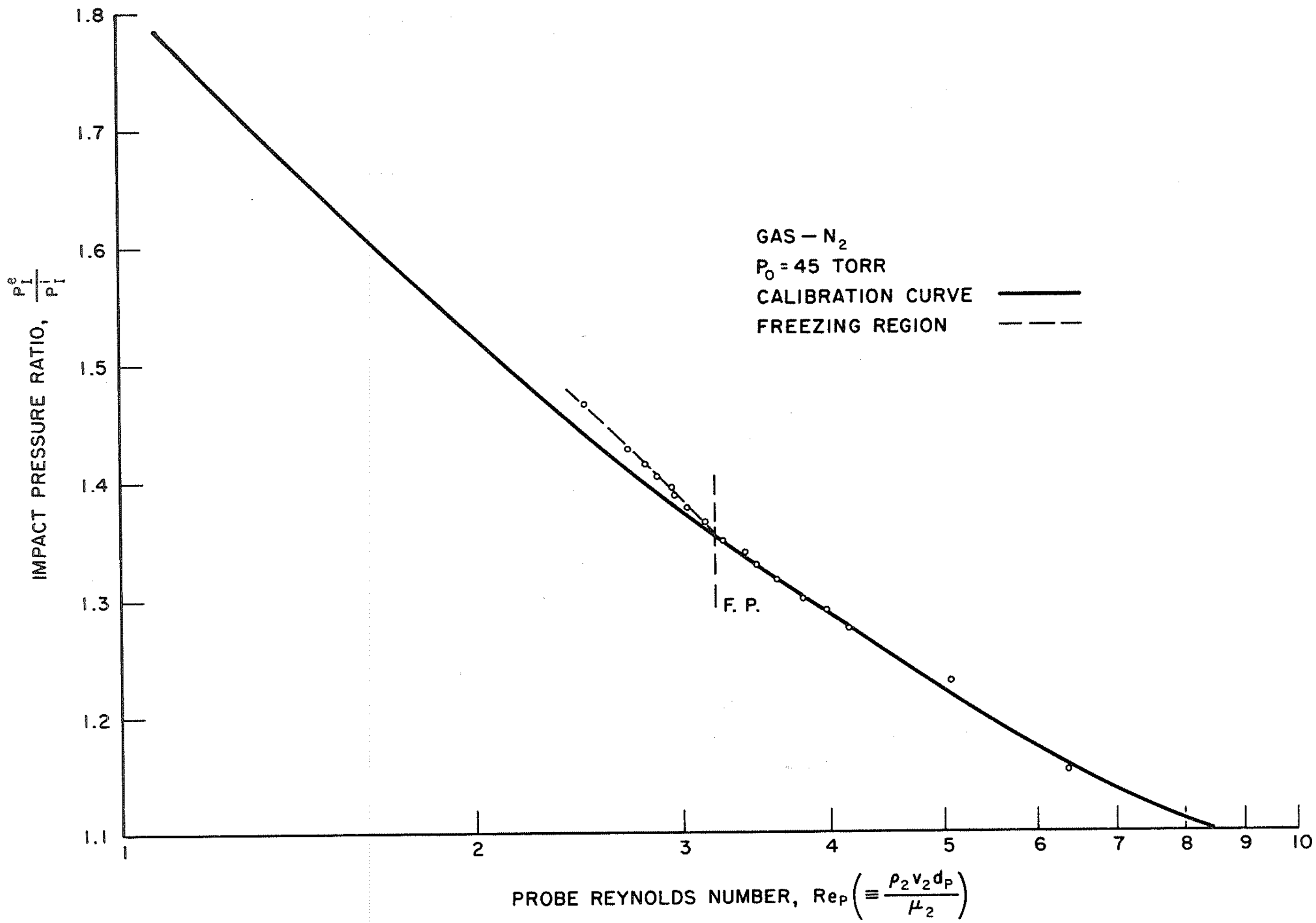

IMPACT-PRESSURE RATIO p_I^e/p_I^i VERSUS
PROBE REYNOLDS NUMBER
(effect of rotational relaxation included)

FIGURE 15

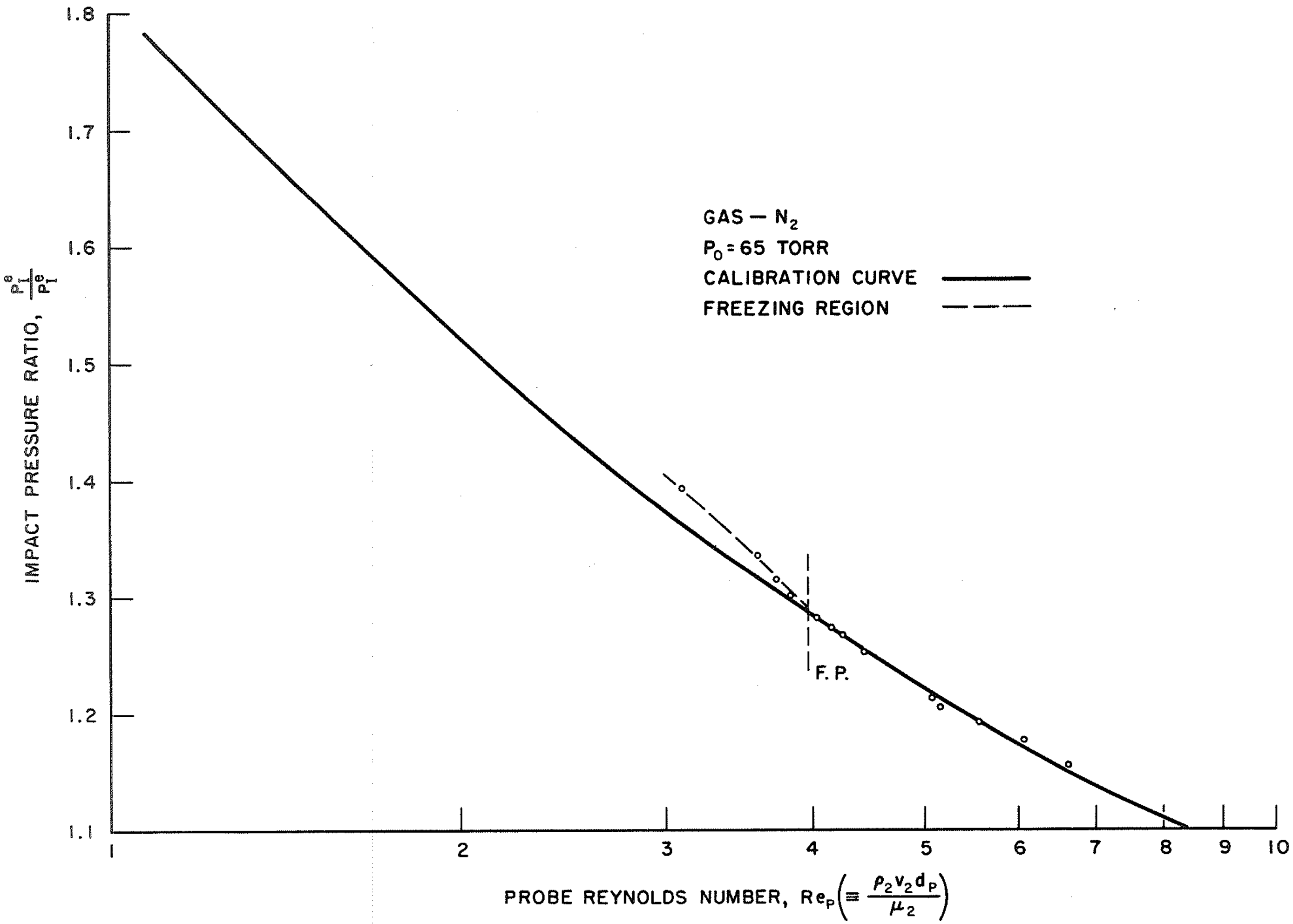

IMPACT-PRESSURE RATIO p_I^e / p_I^i VERSUS
PROBE REYNOLDS NUMBER
(effect of rotational relaxation included)

FIGURE 16

Before undertaking the task of obtaining freezing data, a test was made to determine if in fact the effect of rotational freezing on the impact pressure could be measured. Some doubt had arisen when some investigators reported no difference in measured impact pressure for argon and nitrogen free jets at identical x_p and p_o. The probe was kept at a fixed axial distance from the source while nitrogen and argon were successively admitted at a stagnation pressure of 45 torr. A comparison of measured impact pressure ratios $\left(p_i^e / p_I^i = 0.106 \text{ for } N_2 \text{ and } 0.116 \text{ for Ar}\right)$ at a probe Reynolds number > 25 (negligible viscous effects), showed a significant difference. As a result, the probability of observing an increase in impact pressure as a result of rotational freezing was considered promising.

In Figure 17, the various values of $(x'/D^*)_f$ determined from the impact pressure data are plotted as a function of the dimensionless parameter $D^*/\tau_{ro} a_o$. The number of collisions N_r required for the relaxation is used often to describe the efficiency of rotational energy transfer. It is defined as

$$N_r = \tau_r Z \tag{3}$$

where

$$Z = \left(\frac{8kT}{\pi m}\right)^{1/2} \sqrt{2} \; n \pi r_m^2 \; \Omega_\mu \tag{4}$$

The parameter $D^*/\tau_{ro} a_o$ may be expressed then as

$$\frac{D^*}{\tau_{ro} a_o} = \frac{1}{N_r} \left(\frac{8}{\pi \gamma}\right)^{1/2} \frac{\sqrt{2}\; p_o \pi r_m^2 \Omega_\mu D^*}{k T_o} \tag{5}$$

Using the values obtained in Reference 40 for a Modified Buckingham (6-Exp) Potential, together with $T_o = 296^oK$ and $N_r = 5.3$ (Reference

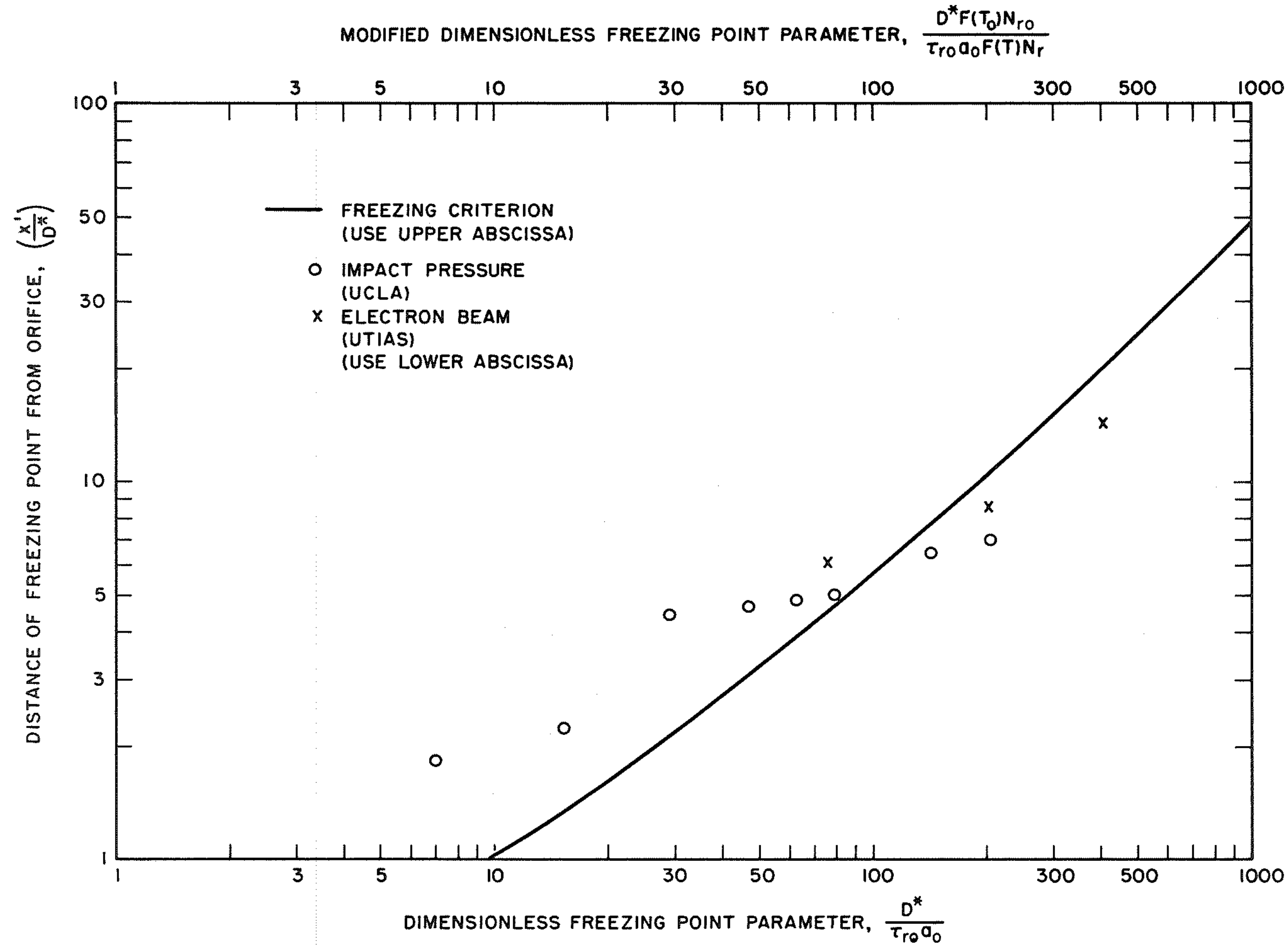

FREEZING-POINT DISTANCE $(x'/D^*)_f$ VERSUS DIMENSIONLESS FREEZING-POINT PARAMETER $(D^*/\tau_{ro} a_o)$

FIGURE 17

41), one may write Equation (5) in the form

$$\frac{D^*}{\tau_{ro} a_o} = 131\, p_o D^* \qquad (6)$$

where $p_o D^*$ has units torr-in. The experimental freezing-point data are compared with the $(x'/D^*)_f$ values predicted using the criterion $\left|\frac{DT}{Dt}\right| = \frac{T}{\tau_r}$. In order to express the distance at which freezing may occur as a function of the freezing-point parameter $D^*/\tau_{ro} a_o$, the freezing-point criterion $\left|\frac{DT}{Dt}\right| = \frac{T}{\tau_r}$ is rewritten in the form (compare Equation (7) with Equation (11) in Reference 11)

$$(\gamma - 1)\, M^2 \left(1 + \frac{\gamma - 1}{2} M^2\right)^{\frac{2-\gamma}{\gamma-1} - \frac{1}{2}} \frac{dM}{d(x/D^*)} = \frac{D^*}{\tau_{ro} a_o} \frac{F(T_o)}{F(T)} \frac{N_{ro}}{N_r} \qquad (7)$$

where the following relations were used

$$\frac{a}{a_o} = \left(1 + \frac{\gamma - 1}{2} M^2\right)^{-1} \qquad \text{(perfect gas)} \qquad (8)$$

$$\frac{n_o}{n} = \left(1 + \frac{\gamma - 1}{2} M^2\right)^{\frac{1}{\gamma-1}} \qquad \text{(perfect gas, isentropic flow)} \qquad (9)$$

$$\frac{1}{T} \frac{dT}{dx} = - \frac{(\gamma - 1)\, M}{1 + \frac{\gamma - 1}{2} M^2} \frac{dM}{dx} \qquad \text{(perfect gas, adiabatic flow)} \qquad (10)$$

$$\frac{\tau_r}{\tau_{ro}} = \frac{n_o}{n} \frac{F(T)}{F(T_o)} \frac{N_r}{N_{ro}} \qquad (11)$$

The function F(T) describes the temperature dependence of Z. For a given gas the left-hand side of Equation (7) is a function of x/D^*

only. A plot of the distance at which freezing occurs as a function of the parameter $\frac{D^*}{\tau_{ro} a_o} \frac{F(T_o)}{F(T)} \frac{N_{ro}}{N_r}$ also is shown in Figure 17. The value of $F(T) N_r / F(T_o) N_{ro}$ may be computed by dividing $D^* / \tau_{ro} a_o$ by $\frac{D^*}{\tau_{ro} a_o} \cdot \frac{F(T_o)}{F(T)} \frac{N_{ro}}{N_r}$ corresponding to a given value of $(x'/D^*)_f$. Also shown in Figure 17 are the freezing points determined from the spectroscopic data of Marrone.[14] The freezing point was determined from Marrone's rotational-temperature distribution by the condition $\frac{dT_r}{d(x/D^*)} = \frac{1}{2} \frac{dT}{d(x/D^*)}$ as suggested by Phinney.[42] This definition is used by Phinney to predict the asymptotic vibrational temperature in an expanding nozzle flow and was compared favorably with the vibrational temperature calculated from the relation $\frac{DT_v}{Dt} = \frac{1}{\tau_v} \left(T_T - T_v \right)$. Using either definition of the freezing point $\left| \frac{DT}{Dt} \right| = \frac{T}{\tau_v}$ or $\frac{dT_v}{d(x/D^*)} = \frac{1}{2} \frac{dT}{d(x/D^*)}$ he is able to predict closely the frozen vibrational temperature. The two definitions are therefore assumed to be equivalent. Except for a slight shift to larger $(x/D^*)_f$, Marrone's data seems to agree with results of the impact pressure measurements.

In Figure 18 the temperature dependence of the function $\frac{G(T_o)}{G(T)} \left[\equiv \left(\frac{T}{T_o} \right)^{1/2} \frac{F(T)}{F(T_o)} \right]$, obtained from the freezing point data as described in the preceding paragraph, is shown. In this calculation, N_r was assumed to be independent of temperature within the range ($T < 100^oK$) corresponding to the experimentally determined freezing points. The data are compared with the straight line

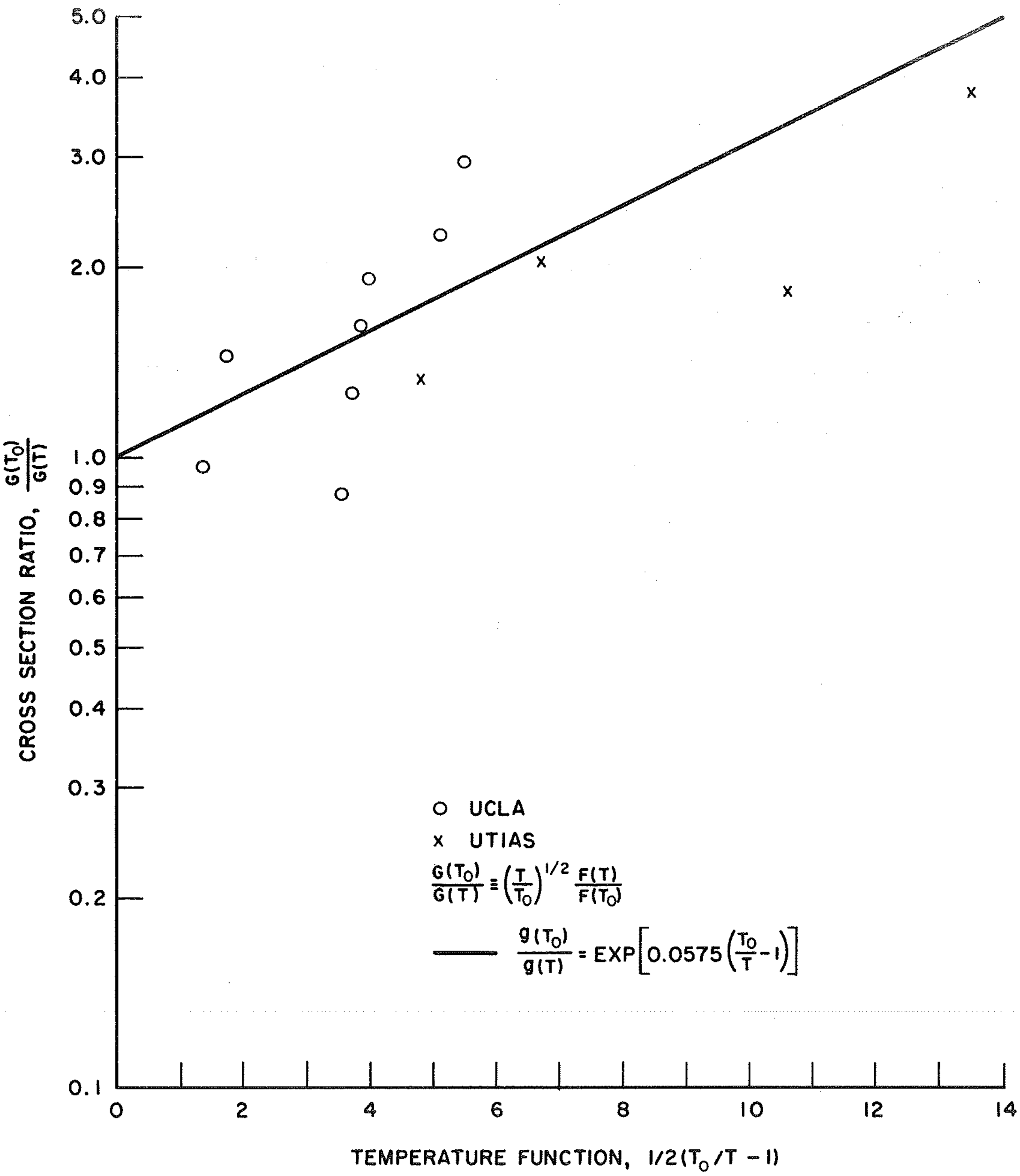

TEMPERATURE DEPENDENCE OF THE COLLISION CROSS SECTION FOR MOLECULES WHOSE CENTERS APPROACH TO 0.993σ OR LESS

FIGURE 18

$\frac{g(T_o)}{g(T)} = \exp .0575\left(\frac{T_o}{T} - 1\right)$. The value of $N_r \sim 1$ ($N_r/N_{ro} = 0.16$) is determined from the condition that $g(T_o)/g(T) = 1$ at the stagnation temperature.

2. Interpretation of results

The relaxation time is the quantity which is related closely to experimental observation. However, for comparing the efficiency of energy transfer of one molecule with another, the relaxation number N_r is a more meaningful quantity. In order to calculate N_r for molecules other than hard spheres, a suitable criterion for a collision which is more relevant for the exchange of energy is required. Rowlinson[43] suggests the rate of collisions be based on a criterion of closeness of approach. For the case where only those collisions are counted for which the centers of molecules approach to less than σ he obtains

$$\bar{Z} = Z \exp\left(-V(r)/kT\right) \qquad (r < \sigma) \tag{12}$$

where

$$Z = 4nr^2 \left(\frac{\pi kT}{m}\right)^{1/2} \tag{13}$$

Then one may write

$$\frac{\bar{Z}}{\bar{Z}_o} = \frac{Z}{Z_o} \exp - \left[\frac{V(r)}{kT_o}\right] \left(T_o/T - 1\right) \tag{14}$$

The collision frequency decreases with temperature more rapidly than a hard sphere model predicts ($\sim T^{1/2}$ at constant density) since low velocity molecules fail to make effective collisions. Now Equation (11) may be written

$$\frac{\tau_r}{\tau_{ro}} = \frac{Z_o}{Z} \; \frac{G(T_o)}{G(T)} \; \frac{N_r}{N_{ro}} \qquad (T < 100) \qquad (15)$$

Substituting the function $g(T_o)/g(T)$ for $G(T_o)/G(T)$, one may write

$$\frac{\tau_r}{\tau_{ro}} = \frac{Z_o}{Z} \; \exp .0575 \left(T_o/T - 1\right) \frac{N_r}{N_{ro}} \quad (T < 100) \qquad (16)$$

Hence, if N_r is constant for $T < 100^oK$, then the relaxation time is determined by a rotational collision number $N_r \sim 1$ and a collision cross section based on closeness of approach with temperature dependence factor $\exp(-.0575\ T_o/T)$. Rotational non-equilibrium effects will be much larger than $N_r \sim 1$ implies due to the inability of molecules with low velocities to make effective collisions. At $T = 10^oK$ for example, $\bar{Z} = .0615Z$ (see Equations (4) and (10)).

Using a Lennard-Jones 6:12 Potential with $\sigma = 3.68\text{Å}$, $\epsilon/k = 91.5^oK$ and $V(r)/kt = 0.0575$ (the value of $V(r)/kt$ was obtained from the slope of the function $g(T_o)/g(T)$ shown in Figure 18 (see Equation (14)), one finds $r = 0.993\ \sigma$ for the distance within which two molecules must approach to make effective collisions.

3. <u>Comparison with other results</u>

In stating that the function $\exp(-.0575\ T_o/T)$, determined from a best fit of the data (Figure 18), gives the temperature dependence of a collision cross section based on closeness of approach, it was assumed that N_r ($\sim$ 1) was constant for $T < 100^oK$. The strength of this assumption rests mainly on the correlation obtained in Figure 18. The scatter in the data appears to be uniform for temperatures of 10-100^oK. The only published experimental results of rotational relaxation numbers obtained from free jet studies is

Miller's data for a two-dimensional source. (The method he used was described in Chapter I-2.) For temperatures less than 200°K, he obtains $N_r \sim 1$. Since this is a lower limit for N_r, it is reasonable to assume that N_r remains constant at this value for temperatures down to 10°K. (It appears odd that N_r should be less than 15/8, the number of collisions which are necessary for translational relaxation.) Miller used a hard-sphere molecular model to calculate the collision frequency. This model corresponds to the closeness-of-approach model for the special case in which the molecules approach to σ or less. In general, other models are required. For example, if the significant collisions are those in which the centers approach to r_M or less, then the relevant collision frequency is similar to that obtained by Sutherland for rigid spheres surrounded by an attractive potential. Hence the type of collision which is counted in a given experiment determines whether a rigid-sphere or a more realistic model is appropriate.

Various estimates of N_r have been obtained from analytical studies of the collisional efficiency of rotational energy transfer. In general, if attractive forces are neglected, then the analyses predict that N_r is independent of temperature. If attractive forces are considered, then the analyses predict that N_r decreases with decreasing temperature. However, the latter predictions are questioned since the kinetic collision frequency is obtained from a model which is inconsistent with the molecular model used in considering the rotational energy transfer. Specifically, either a hard sphere cross section or a cross section of the type $\sigma^2 \Omega_{\mu}$ is used in the calculations of kinetic collision frequency. Recently, Sather and Dahler[44] obtained a rotational collision number for a spherocylinder molecular model. They used a kinetic collision frequency which was consistent with the molecular model and found N_r independent of temperature.

An N_r which is independent of temperature may have been predicted also using Ehrenfest's principle. It suggests that a collision is nearly adiabatic if its duration is much greater than the period of the energy mode being excited $(h/\Delta E)$. The rotational collision number may be considered to be proportional to the ratio of collision duration to the period of molecular rotation. Since the latter two quantities are both proportional to $T^{-1/2}$ (Reference 4), N_r is independent of temperature.

A comparison of the results obtained using the freezing criterion $\left|\frac{DT}{Dt}\right| = \frac{T}{\tau_r}$ with the results of the more detailed theory of Hamel and Willis[45] shows reasonably good agreement. They obtain solutions for a set of closed moment equations derived from the Boltzmann equation for source flow. Fair agreement with Marrone's data was obtained by assuming N_r is constant and using a viscosity cross section which decreases with decreasing temperature. However, viscosity measurements indicate that a more realistic dependence of the viscosity cross section on temperature should be $\sigma^2 \Omega_\mu \sim T^{-1/3}$. (See e.g., Reference 40.) A temperature dependence similar to that obtained by Hamel and Willis for $\sigma^2 \Omega_\mu$ has been obtained also from the impact-pressure data (see Equation 16). This result is interpreted, however, using the closeness-of-approach criterion rather than an unusual temperature dependence of the viscosity cross section.

Hamel and Willis compared the temperature at which freezing takes place as predicted by the freezing criterion $\left|\frac{DT}{Dt}\right| = \frac{T}{\tau_r}$ with the asymptotic value of the rotational temperature calculated from the equation $\frac{DT_r}{Dt} = -\frac{T_r - T_T}{\tau_r}$. For the range of N_r from 2 to 21, and s from 1 to 0.5 (where $\mu \sim T^s$), their results appear to be within 50% of the correct values. Since the results are shown to be more accurate for small s ($\sim$ 10% at N_r = 2.1 and s = .5), predictions made using this freezing criterion to obtain freezing temperatures in a free jet of nitrogen should fall within this limit.

The rotational relaxation number obtained by probing a free jet might not correspond to that obtained from shock-tube or ultrasonic-dispersion data. At room temperature, Miller found $N_r = 3$ whereas ultrasonic and shock tube data indicated $N_r = 6$. A similar discrepancy has been observed for vibrational relaxation of nitrogen in supersonic nozzle flows (References 18, 23, 46). Since various methods have been used to probe the free-jet flow (e.g., static-pressure probe, fluorescence techniques, and electron-beam excitation), a deficiency in the method does not appear to be responsible.

The drain of rotational energy via the lower energy states might be faster in free-jet flows than in shock-wave or ultrasonic-dispersion experiments. The closer spacing of the lower rotational energy levels facilitates conversion of several smaller rotational quanta to translational energy in a single collision. Rotational energy is dissipated faster this way than by the loss of one large quantum on collision (Reference 47). Also, the molecules in higher rotational energy states might share most of their rotational energy on collision rather than lose it completely to translation. This type of process would be more significant though for molecules whose atoms have a large mass ratio.

Some information concerning the relaxation of individual rotational levels can be obtained from spectroscopic data. The observed intensities of the rotational peaks are generally plotted semi-logarithmically as a function of rotational quantum number (as in Reference 14). An equilibrium rotational energy distribution yields a straight line with slope inversely proportional to the rotational temperature. A discontinuity in the slope corresponds to two distinct distributions of rotational energy, one at a high temperature (large K) and one at a lower or "normal" temperature, indicating a slower relaxation of the upper rotational levels. Such a discontinuity has been observed in a spectroscopic study of an acetylene-oxygen flame (Reference 48).

Marrone's data shows the same effect. He suggests it is due to the rapid expansion of the nitrogen free jet. Ashkenas[49] later made low-temperature measurements in a static gas and found a nonequilibrium rotational energy distribution. The excitation-emission model of Muntz appears to be inadequate.

The relaxation may be governed by the thermodynamic process which is involved. However, for diatomic gases, the differences between the several possible relaxation numbers are only a few percent (Reference 3). Such differences would not account for the large difference in the relaxation number obtained from free-jet studies and the numbers obtained from shock-tube and ultrasonic data.

CHAPTER V

SUMMARY OF RESULTS AND CONCLUSIONS

1. Summary

An extensive impact-pressure survey was made of a free jet of nitrogen. The results which were obtained, and the conclusions based on the preceding discussion of the data, are presented here.

1. Effects of rotational nonequilibrium were observed using a pitot tube. The impact pressure is found to deviate from the predictions of inviscid theory for free jets (after corrections for shock detachment, nozzle boundary layer, and viscous effects at the probe) at larger Mach numbers as the source pressure is increased. The corrected data scattered approximately 1/2% relative to predictions for inviscid flow.

2. The rotational-relaxation time at low temperatures ($< 100^oK$), inferred from the impact pressure data by the use of the criterion for sudden freezing $\left| \frac{DT}{Dt} \right| = \frac{T}{\tau_r}$, was expressed by $\frac{\tau_r}{\tau_{ro}} = \frac{Z_o}{Z} \exp .0575 \left(\frac{T_o}{T} - 1 \right)$, where $Z = 4n\sigma^2 \left(\frac{\pi k T}{m} \right)^{1/2}$.

3. The relaxation process was interpreted using a relaxation model in which (a) N_r is constant with value unity over the range from 10^oK to 100^oK and (b) the collision frequency includes only those collisions for which $r \leq 0.993\sigma$. The temperature dependence of the collision frequency for this model is significantly different than the rate based on a viscosity cross section.

4. Pitot-tube corrections were obtained for probe Reynold's numbers from 1 to 10.

5. The discharge characteristics of a round-edged orifice were obtained for sonic Reynold's numbers from 100 to 1400.

6. Effective source location corrections were obtained for sonic Reynold's numbers from 100 to 1000.

7. Significant differences in measured impact pressure (10%) for argon and nitrogen free jets were observed at identical stagnation pressure and nozzle-to-probe distance.

2. Conclusions

The freezing criterion $\left|\frac{DT}{Dt}\right| = \frac{T}{\tau_r}$ may be used profitably to define the point at which rotational relaxation effects in a free jet may be detected by a pitot tube, thereby allowing the determination of the rotational relaxation time.

A relaxation model in which N_r is constant and the collision frequency is fixed by a closeness-of-approach criterion is consistent with the observed relaxation times.

BIBLIOGRAPHY

1. Jeans, James H., Dynamical Theory Of Gases, New York, Cambridge University Press, 1904.
2. Pierce, G. W., Proc. Amer. Acad., 60:271, 1925.
3. Cottrell, Tom L. and J. C. McCoubrey, Molecular Energy Transfer In Gases, London, Butterworths, 1961.
4. Mason, Warren P., Physical Acoustics, Principles and Methods, New York, Academic Press, 1965.
5. Herzfeld, Karl F., and Theodore A. Litovitz, Absorption and Dispersion of Ultrasonic Waves, New York, Academic Press, 1959.
6. Kantrowitz, A., and J. Grey, "High Intensity Source for the Molecular Beam, Part I, Theoretical," Rev. Sci. Inst., 22:328-332, May 1951.
7. Kantrowitz, A., "Heat-Capacity Lag In Gas Dynamics," J. Chem. Phys., 14:150-164, March 1946.
8. Huber, H. H., and A. Kantrowitz, "Heat-Capacity Lag Measurements In Various Gases," J. Chem. Phys., 15:275-284, May 1947.
9. Reis, R. H., "Free Expansion Of Pure And Mixed Gases From Small Sonic Nozzles," Princeton U., Report No. FLD-7, May 1962.
10. Knuth, E. L., "Rotational And Translational Relaxation Effects In Low-Density Hypersonic Free Jets," U. of California (Los Angeles) Report No. 64-53, November 1964.
11. Knuth, E. L., "Supersonic Molecular Beams," Applied Mechanics Reviews, 17:751-762, October 1964.
12. Muntz, E. P., S. J. Abel and B. L. Maguire, "The Electron Beam Fluorescence Probe In Experimental Gas Dynamics," IEEE Conference on Aerospace, Houston, Texas, July 1965.
13. Muntz, E. P., "Measurement Of Rotational Temperature, Vibrational Temperature, And Molecule Concentration, In Non-Radiating Flows Of Low Density Nitrogen," U. of Toronto, UTIAS Report No. 71, April 1961.

14. Marrone, P.V., "Rotational Temperature And Density Measurements In Underexpanded Jets And Shock Waves Using An Electron Beam Probe." U. of Toronto, UTIAS Report No. 113, January 1966.

15. Robben, F., and L. Talbot, "Some Measurements Of Rotational Temperatures In A Low Density Wind Tunnel Using Electron Beam Fluorescence," U. of California (Berkeley) Report No. AS-65-5, May 1965.

16. Hickman, R.S., "Rotational Temperature Measurements In Nitrogen Using An Electron Beam," U. of Southern California, USCAE Report No. 104, September 1966.

17. Yasuhara, M., "Rotational Temperature Measurement Of The Flow Expanding From A Low Density Sonic Orifice," U. of Southern California, USCAE Report No. 103, August 1966.

18. Hurle, I.R., A.L. Russo, and J.G. Hall, "Spectroscopic Studies Of Vibrational Nonequilibrium In Supersonic Nozzle Flows," J. Chem. Phys., 40:2076-2089, April 1964.

19. Hagena, O. and W. Henkes, "Untersuchung der Thermischen Relaxation Bei Düsenströmugen Durch Analyse der Gaskin-etishen Geschwindigkeitsverteilung," Z. für Naturforschung, 15a:851-858, October 1960.

20. Miller, David R., Rotational Relaxation Of A Diatomic Molecule, Ph.D. Thesis, Dept. of Chem. Engr., Princeton U., New Jersey, January 1960.

21. Campargue, R., "Relaxation Phenomena In The Generation Of Supersonic Molecular Beams," Molecular Relaxation Processes, New York, Academic Press, 1966.

22. Bier, K., and B. Schmidt, "Zur Form der Verdichtungs-stösse In Frei Expandierenden Gasstrahlen," Z. für ange-wandte Physik., 13:493-500, November 1961.

23. Duffy, R.F., "A Static Pressure Measurement Technique For Chemical Kinetic Studies," Proceedings of the First Internat. Congress Instrumentation In Aerospace Facilities, Paris, France, September 1964.

24. Owen, P.L., and C.K. Thornhill, "The Flow In An Axially-Symmetric Supersonic Jet From A Nearly-Sonic Orifice Into A Vacuum," Aeronautical Research Council, R and M 2616, September 1948.

25. Ashkenas, H., and F.S. Sherman, "The Structure And Utilization Of Supersonic Free Jets In Low Density Wind Tunnels," Rarefied Gas Dynamics, Vol. I, New York, Academic Press, 1966.

26. Reis, V.H. and J.B. Fenn, "Separation Of Gas Mixtures In Supersonic Jets," J. Chem. Phys., 39:3240-3250, December 1963.

27. Fenn, J.B. and J. Deckers, "Molecular Beams From Nozzle Sources," Rarefied Gas Dynamics, Vol. I, New York, Academic Press, 1963.

28. Stollery, J.L. and J.E. Smith, "A Note On The Variation Of Vibrational Temperature Along A Nozzle," J. Fluid Mech., 13:225-236, June 1962.

29. Bray, K.N.C., "Atomic Recombination In A Hypersonic Wind Tunnel," J. Fluid Mech., 6:1-32, July 1959.

30. Phinney, R., "Criterion For Vibrational Freezing In A Nozzle Expansion," AIAA J., 1:496-497, February 1963.

31. Schaaf, S.A. and R.R. Cyr, "Time Constants For Vacuum Gage Systems," J. of Appl. Phys., 20:860-863, September 1949.

32. Knuth, E.L., "Second Status Report On Development And Application Of An Intermediate-Energy High-Intensity Molecular Beam," U. of California (Los Angeles) Report No. 66-19, April 1966.

33. Liepmann, Hans W. and Anatol Roshko, Elements Of Gas Dynamics, New York, Wiley, 1960.

34. Wang, C.J., J.B. Peterson and A. Anderson, "Gas Flow Tables," Space Technology Laboratories, Inc., GM-TR-154, March 1957.

35. Serbin, H., "The High Speed Flow Of Gas Around Blunt Bodies," The Aeronautical Quarterly, 9:313-330, November 1958.

36. Anderson, J.B., R.P. Andres, J.B. Fenn and G. Maise, "Studies Of Low Density Supersonic Jets," Rarefied Gas Dynamics, Vol. II, New York, Academic Press, 1966.

37. Homann, F., "The Effect Of High Viscosity On The Flow Around A Cylinder And Around A Sphere," National Advisory Committee For Aeronautics, Technical Note, NACA-TN-1344, June 1952.

38. Chambre, P. L., "The Theory Of The Impact Tube In A Viscous Compressible Gas," U. of California (Berkeley) Report No. HE-150-50, November 1958.

39. Sherman, F. S., "New Experiments On Impact-Pressure Interpretation In Supersonic And Subsonic Rarefied Air Streams," National Advisory Committee For Aeronautics, Technical Note, NACA-TN-2995, September 1953.

40. Hirschfelder, Joseph O., Charles F. Curtiss and Robert B. Bird, Molecular Theory Of Gases And Liquids, New York, Wiley, 1954.

41. Greenspan, M., "Relaxation In Nitrogen, Oxygen, And Air," J. Acoust. Soc. Amer., 31:155-160, February 1959.

42. Phinney, R., "Mathematical Nature Of The Freezing Point In An Expanding Flow," Martin Marietta Co. (Baltimore), RM-172, April 1964.

43. Rowlinson, J. S., "The Rate Of Molecular Collisions In Gases Composed Of "Soft" Molecules," Molecular Physics, 4:317-320, April 1961.

44. Sather, N. F. and J. S. Dahler, "Molecular Friction In Dilute Gases, II, Thermal Relaxation Of Translational And Rotational Degrees Of Freedom," J. Chem. Phys., 35:2029-2037, December 1961.

45. Hamel, B. B. and D. R. Willis, "Nonequilibrium Effects In Spherical Expansions Of Polyatomic Gases And Gas Mixtures," Rarefied Gas Dynamics, Vol. I, New York, Academic Press, 1966.

46. Sebacher, D.I. and R. J. Duckett, "A Spectrographic Analysis Of A 1-foot Hypersonic Arc Tunnel Airstream Using An Electron Beam Probe," National Aeronautics and Space Administration, Technical Report, NASA-TR-R-214, December 1964.

47. Oldenberg, O. and A. A. Frost, "Molecular Translation, Rotation, And Vibration In Chemical Activation," Chem. Rev., 20:99-129, December 1936.

48. Gaydon, A. G. and H. G. Wolfhard, "Spectroscopic Studies Of Low-Pressure Flows; Temperature Measurements In Acetylene Flames," Proc. Roy. Soc., 194A:169-184, August 1948.

49. Ashkenas, H., "On Rotational Temperature Measurements In Electron Beam Excited Nitrogen," Submitted for publication.